Tectonics

RESEARCH ARTICLE
10.1029/2017TC004903

Key Points:
- The diverse rift-related structural domains in the margin have distinctive gravity anomaly imprints
- Mapping of the crustal and structural domains shows a strong segmentation of the NW Iberia margin with high inheritance control
- Rift architecture and segmentation control the development of the partial tectonic inversion of the margin

Supporting Information:
- Supporting Information S1
- Figure S1
- Figure S2

Correspondence to:
M. Druet,
m.druet@igme.es

Citation:
Druet, M., Muñoz-Martín, A., Granja-Bruña, J. L., Carbó-Gorosabel, A., Acosta, J., Llanes, P., & Ercilla, G. (2018). Crustal structure and continent-ocean boundary along the Galicia continental margin (NW Iberia): Insights from combined gravity and seismic interpretation. *Tectonics*, *37*, 1576–1604. https://doi.org/10.1029/2017TC004903

Received 29 NOV 2017
Accepted 8 APR 2018
Accepted article online 20 APR 2018
Published online 27 MAY 2018

Crustal Structure and Continent-Ocean Boundary Along the Galicia Continental Margin (NW Iberia): Insights From Combined Gravity and Seismic Interpretation

M. Druet[1,2], A. Muñoz-Martín[2], J. L. Granja-Bruña[2], A. Carbó-Gorosabel[2], J. Acosta[3], P. Llanes[2], and G. Ercilla[4]

[1]Instituto Geológico y Minero de España, Madrid, Spain, [2]Applied Tectonophysics Group, Departamento de Geodinámica, Universidad Complutense de Madrid, Madrid, Spain, [3]Instituto Español de Oceanografía, Madrid, Spain, [4]Institut de Ciènces del Mar, CSIC. Grup de Marges Continentals, Barcelona, Spain

Abstract The magma-poor rifted continental margin of Galicia has an extremely complex structure. Its formation involved several rifting episodes that occurred ultimately during the early Cretaceous near a ridge triple junction, which produced a change in the orientation of the main structures in its transition to the north Iberia margin. In addition, there is a superimposed partial tectonic inversion along its northwest and northern border which developed from the Late Cretaceous to at least Oligocene times. The present study integrates a large volume of new geophysical information (mainly marine gravity data and 2-D seismic reflection profiles) to provide insights on the formation of this rift system and on the development of its later inversion. The combined interpretation and modeling of this data enable the presentation of a new crustal and structural domain map for the whole Galicia margin. This includes the rift domains related to the extreme thinning of the crust and the lithospheric mantle (stretched, necking, and hyperextension and mantle exhumation domains), as well as a domain of intense compressional deformation. New constraints arise on the origin, the deep structure, and the characterization of the along- and across-strike variation of the continent-ocean transition of the margin, where a progressive change from hyperextension to partial inversion is observed. The development of both rifting and later partial tectonic inversion is influenced by the existence of former first-order tectonic features. Most of the tectonic inversion is focused on the hyperextension and mantle exhumation domain, which in some areas of the northwestern margin is completely overprinted by compressional deformation.

1. Introduction

The understanding of the development of magma-poor rifted margins and their behavior under a subsequent compressional tectonic regime has been in the spotlight during the last years. Recent models are based on the study of different domains, typically seaward arranged, that originated during the rifting. A good deal of these studies have been developed along the Iberia margins and its conjugates (e.g., Lavier & Manatschal, 2006; Péron-Pinvidic et al., 2013; Stanton et al., 2016; Tugend et al., 2014). This rift domain mapping allows the interpretation of distinct stages of their formation, illustrating the margin evolution as well as the behavior of each domain during tectonic reactivation (e.g., Tugend et al., 2014). New concepts and definitions have been developed, but there is still a relative variability about the nomenclature and delineation of boundaries between domains (Chenin et al., 2017; Péron-Pinvidic et al., 2013; Sutra et al., 2013; Tugend, Manatschal, Kusznir, et al., 2015).

Although some detailed rift-related domain mapping has been previously interpreted on the west Iberia margin (Péron-Pinvidic et al., 2013), and on the north Iberia margin (Tugend et al., 2014), there is a gap on this domain mapping on the assembly between both margins, that is, on the (northwest) Galicia margin. The aim of this work is to analyze the structural framework of the whole Galicia margin, from west to north. A detailed analysis of gravity data and 2-D reflection seismic profiles, accompanied by 2+3/4−D gravity models serially arranged across the main features of the margin, provide information on its the deep crustal structure. The newly mapped rift domains and the observations made on the deep structure of the margin throw light on the way the transition from the west to the north Iberia margins takes place, as well as on the influence of the rift architecture on its later partial inversion.

1.1. Terminology

All magma-poor rifted margins have some common architectural features (e.g., Reston, 2009), with an outstanding succession of different domains that relate to specific deformation processes (e.g., Naliboff et al., 2017; Péron-Pinvidic et al., 2013; Sutra et al., 2013; Tugend et al., 2014). The boundaries between these rift domains are sometimes diffuse, as deformation processes may overlap in time and space (e.g., Tugend, Manatschal, Kusznir, et al., 2015). There is a relatively wide range of rift domain definitions (e.g., Chenin et al., 2015; Péron-Pinvidic et al., 2013; Stanton et al., 2016; Sutra et al., 2013; Tugend et al., 2014), and the criteria for the identification of their limits may differ. The terminology used in this study is adapted from those previously published (e.g., Chenin et al., 2015; Péron-Pinvidic et al., 2013; Sutra et al., 2013; Tugend et al., 2014), in order to account for the special characteristics of the Galicia margin, which are described further down. The terminology adopted here is as follows.

1.1.1. Stretched Domain

This domain corresponds to the *proximal domain* described by Péron-Pinvidic et al. (2013) and to the *stretched domain* defined by Sutra et al. (2013). This region is moderately affected by crustal thinning (Péron-Pinvidic & Manatschal, 2009), and basement top and the Moho are approximately parallel. Deformation is decoupled, with brittle faulting at the upper part of the crust and a ductile behavior of the lower continental levels, separated by a brittle/ductile transition (decoupling level, Sutra et al., 2013). Due to the moderate thinning, little accommodation space is created (Sutra et al., 2013).

1.1.2. Necking Domain

In this region, the crust is wedge-shaped and records a thinning until reaching 10 km of crustal thickness (Mohn et al., 2015; Péron-Pinvidic & Manatschal, 2009). Moho inflects and rises, tending to converge with the dipping continental basement top, and much more accommodation space is created than in the stretched domain (Péron-Pinvidic et al., 2013; Péron-Pinvidic & Manatschal, 2009). Here crustal deformation is still decoupled (Sutra et al., 2013). The distal border of this domain is located where the crustal thickness is less than 10 km thick, and an embrittlement of the whole crust occurs (Péron-Pinvidic et al., 2013; Pérez-Gussinyé & Reston, 2001; Pérez-Gussinyé et al., 2003; Sutra et al., 2013).

1.1.3. Hyperextension and Mantle Exhumation Domain

Along this distal domain, crustal thickness is less than 10 km and the tectonic deformation is coupled. Extensional faulting penetrates and exhumes the continental lithospheric mantle under a simple shear regime (Doré & Lundin, 2015; Pérez-Gussinyé et al., 2003; Sutra et al., 2013), and serpentinization of the lithospheric mantle occurs (Pérez-Gussinyé & Reston, 2001). As tectonic thinning progresses, the serpentinized mantle is exposed and is in direct contact with the sedimentary cover or may crop out to the seafloor (e.g., Boillot, Comas et al., 1988; Boillot, Winterer et al., 1988; Sutra et al., 2013, and references therein).

2. Regional Setting

The Galicia margin, as the rest of the west and north Iberia margin, originated from the northward propagation of the Atlantic Ocean opening from Late Jurassic to Early Cretaceous times (e.g., Murillas et al., 1990). This rift episode affecting Iberia culminated with the breakup of the conjugate margin pairs of Galicia-Flemish Cap (the northern sectors of the west Iberia-Newfoundland conjugate margins; e.g., Sutra et al., 2013, and references therein) and the opening of the Bay of Biscay, with the separation of the north Iberia-Armorica-Celtic conjugate margins (e.g., Tugend et al., 2014, and references therein). These conjugate margin pairs of west and north Iberia were connected by a triple ridge junction located to the northwest of Galicia. The kinematics of this triple junction initiation is strongly debated, and different models are proposed for the Bay of Biscay opening, ranging from a transtensional model, to a scissor-type opening (e.g., Jammes et al., 2009; Mouthereau et al., 2014; Olivet, 1996; Sibuet & Collette, 1991; Sibuet, Srivastava et al., 2004; Srivastava et al., 2000).

Along-strike segmentation on the west Iberia margin has been related to the staged progression of the North Atlantic opening (e.g., Alves et al., 2009; Brune et al., 2014; Malod & Mauffret, 1990; Srivastava et al., 1990). This segmentation of the western margin is favored by the existence of NW-SE and NE-SW fractures that have been considered either as inherited from the Late Hercynian fabric (e.g., Boillot & Malod, 1988; Manatschal et al., 2015; Martínez Catalán et al., 2009; Murillas et al., 1990; Sibuet et al., 1987) or originated during the Late Triassic-Early Jurassic rift event (e.g., Vegas et al., 2016). On the Galicia sector, the succession of time-

separated rifting pulses leads also to a westward jump of the rift axis, due to lithospheric rheological changes (Manatschal & Bernoulli, 1999). North of Iberia, recent studies point to a rift partition of the margin in different left-lateral transtensional rift systems, where NNE-SSW transfer faults (e.g., Pamplona transfer zone and Santander soft transfer zone), probably originated during Triassic times (e.g., De Vicente & Vegas, 2009; Sopeña et al., 1988; Ziegler, 1982), play a major part during rifting (Jammes et al., 2009; Roca et al., 2011; Tugend, Manatschal, & Kusznir, 2015). The oceanic crust accretion continued in the Bay of Biscay until Santonian times (Srivastava et al., 1990). Afterward, the roughly N-S compressional tectonic stress field taking place during the Alpine orogeny (since the Late Santonian to Oligocene-Miocene times; e.g., Capote et al., 2002; Thinon et al., 2001; Tugend, Manatschal, & Kusznir, 2015) leads to the reactivation and partial inversion of previous rift structures, and some new compressional structures were also generated, such as thrusts, reverse faults, folds, and flexures (e.g., Grimaud et al., 1982; Murillas et al., 1990; Tugend et al., 2014; Vázquez et al., 2008).

As a result of this complex tectonic history, the present-day Galicia continental margin shows an intricate structure. Thereby, the upper continental slope imaged on the Galicia margin comprises different geomorphologic provinces, which are as follows (Figure 1a): The marginal platform region northwest of Galicia (MPR), the Galicia interior basin (GIB), the seamount region (SR), and the deep Galicia margin (DGM). The lower continental slope is steep at the northwestern flank of the SR (Ercilla et al., 2008), as well as bordering the MPR and to the north Iberia margin. The GIB is located westward of the Galician continental shelf, trending NNW-SSE, with an approximated width of 100 km. In this basin, great NNW-SSE normal faults stand out, delineating narrow and elongated continental basement blocks, mainly tilted during the Berriasian-Valanginian rifting stage (Murillas et al., 1990; see Figure 1d), and offset by NE-SW and NW-SE faults. The sedimentary infill reaches a thickness of 6 km in the center of the basin, thinning toward the continental shelf and the SR (Murillas et al., 1990; Pérez-Gussinyé et al., 2003; see Figure 1d). Westward of the GIB, the SR is constituted by a series of continental crust blocks, tilted during the Early Cretaceous rifting and raised later as a consequence of the Pyrenean (Campanian to Oligocene) compressional tectonics (e.g., Boillot & Malod, 1988). This region limits toward the west on the DGM, where it has been identified a band up to few tens of kilometers width, constituted by extremely extended continental crust blocks with a thin sedimentary cover, and underlined by an ultramafic basement (see Figure 1c); this region ends westward in a serpentinized peridotite ridge (Boillot et al., 1987). This ultramafic basement is originated by subcontinental mantle exposure during the final rifting (Kornprobst & Chazot, 2016; Krawczyk et al., 1996). Oceanward from the DGM, a transition from a thin oceanic crust, underlined by serpentinized mantle, to the normal oceanic crust of the Iberia abyssal plain (IAP) is observed (e.g., Davy et al., 2016; Sibuet et al., 1995). To the northwest of Galicia, the MPR seems to be constituted by graben basins originated during the Mesozoic rifting (probably prior to Late Aptian times), as observed in other basins on the north Iberia margin and in the conjugate Armorican margin (Thinon et al., 2003; Tugend, Manatschal, & Kusznir, 2015), and tectonically inverted under the subsequent Santonian to Oligocene compressional regime (Murillas et al., 1990; Thinon et al., 2001; Tugend, Manatschal, & Kusznir, 2015). Oceanward from the MPR and the north of Galicia, an abrupt transition to the oceanic crust is noticed (Álvarez-Marrón et al., 1997; Fernández-Viejo et al., 1998; Tugend et al., 2014).

3. Materials and Methods

Data used in this work come from diverse sources. Offshore, gravity data set was obtained during seven surveys, carried out between 2001 and 2009 northwest of Iberia, onboard the R/V *Hésperides*, within the frame of the Oceanographic and Hydrographic Research Project of the Spanish Economic Exclusive Zone. During these cruises, more than 400,000 ship gravity data points were obtained (Figure 2). Where ship gravity information is not available, the satellite altimetry-derived Global Gravity Model data (version 23.1) have been used (Sandwell et al., 2014). On land, gravity data have been taken from the databases of the "Instituto Geográfico Nacional," the "Empresa Nacional de Residuos Radiactivos," and the "Bureau Gravimétrique International." The gravity meter employed on the data acquisition during the sea surveys is a marine gravimeter Bell Aerospace BGM-3. These data were tied to the on land gravity network on the first-order gravity bases of the Instituto Geográfico Nacional in Cartagena, Santander, Vigo and La Coruña, using a Lacoste and Romberg (model G) gravimeter. The reduction has been executed with the IGRS67, and the final Bouguer anomaly information includes sea-bottom correction (Carbó et al., 2003;

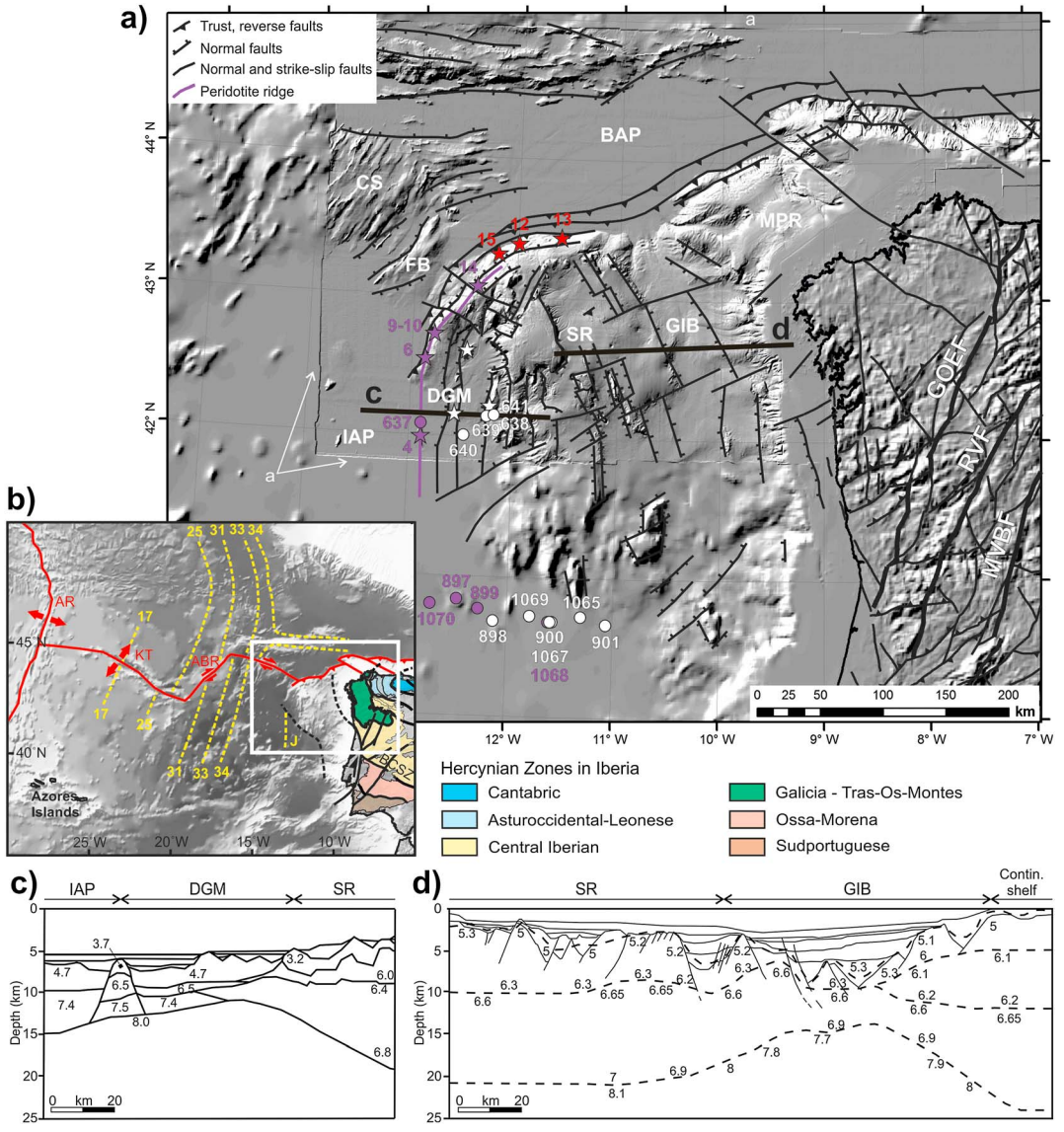

Figure 1. (a) Structural sketch of Northwest Iberia, over the digital terrain model (DTM) obtained by the combination of ship data and the GEBCO Digital Atlas. Modified from Groupe Galice (1979), Boillot, Comas et al. (1988), Boillot et al. (1995), Grimaud et al. (1982), Boillot and Malod (1988), Murillas et al. (1990), Malod et al. (1993), Álvarez-Marrón et al. (1997), Ramírez et al. (2006), and Vázquez et al. (2008). BAP, Biscay abyssal plain; MPR, marginal platform region; CS, Coruña seamounts; FB, Finisterre bank; SR, seamount region; DGM, deep Galicia margin; GIB, Galicia interior basin; IAP, Iberia abyssal plain; GOEF, Guimaraes-Orense-Eo fault; RVF, Regua-Verín fault; MVBF, Manteigas-Vilariça-Bragança fault; a, artifact on the DTM by the ship and GEBCO assemblage. The labeled circles show locations of DSDP and ODP drill holes (Groupe Galice, 1979; Boillot, Winterer et al., 1988; Whitmarsh, Beslier, & Wallace, 1998), whereas the stars show locations of dredge sampling (Boillot, Comas et al., 1988). The purple locations indicate sampling of the exhumed mantle (serpentinite and serpentinized peridotite), while the red locations indicate sampling of oceanic basement rocky outcrops. The white locations indicate either that continental basement was sampled or that the sampling did not reach the basement. (b) Regional map with location of the study area (white rectangle), main fracture zones and plate boundaries during Eocene times (red solid lines), magnetic anomalies on the oceanic domain (yellow dashed lines), and colored, tectono-metamorphic zonation of the Hercynian belt in Iberia (Pérez-Estaún & Bea, 2004), with some of their offshore prolongations (black dashed lines), based on Capdevila and Mougenot (1988), Martínez Catalán et al. (2009), and Manatschal et al. (2015). AR, Atlantic ridge; KT, King's trough; ABR, Azores-Biscay rise; BCSZ, Badajoz-Córdoba shear zone. (c) Refraction seismic velocity model on the continent-ocean transition, modified from Sibuet et al. (1995). (d) Refraction seismic velocity model on the GIB and geological interpretation, modified from Pérez-Gussinyé et al. (2003). Seismic velocity unit on (c) and (d) is km/s.

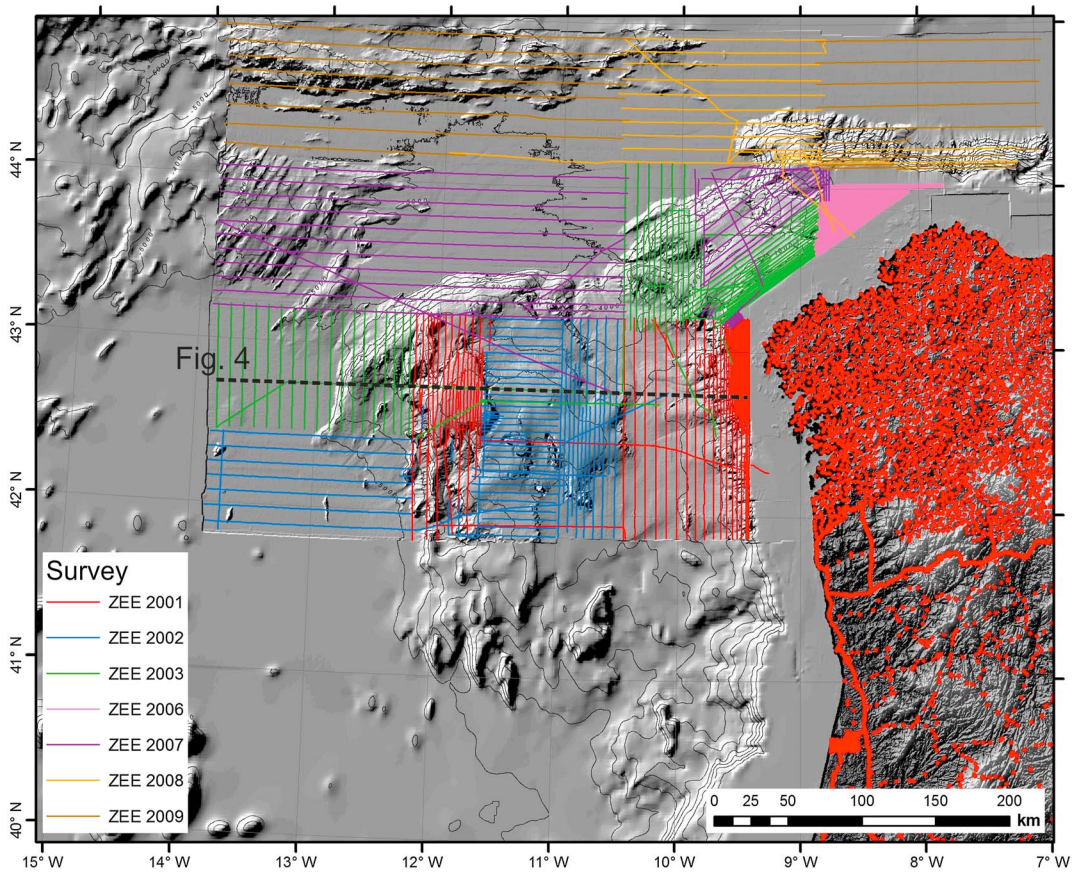

Figure 2. Shaded relief model from the digital terrain model of the study area showing ship navigation lines with gravity (and swath bathymetry) data acquisition during the different surveys. On land, the red points indicate the positions of the gravity measure stations. The black dashed line shows the location of the bathymetric and free-air anomaly profiling extracted for the coherency analysis (Figure 4).

Kane, 1962; Naggy, 1966). Bouguer correction is calculated for a reduction density of 2.67 g/cm^3, and the topographic correction has been carried out up to 22 km, using a 2-km-gridded digital terrain model (Sandwell et al., 2014). Finally, ship gravity data, on land information and that derived from satellite altimetry, were jointly processed and included in a georeferenced database. This data set was interpolated to obtain a 2-min regular grid for the Bouguer anomaly values. In addition to the gravity data, several original multichannel reflection seismic profiles across northwestern flank of the SR were available. These were collected in the frame of the ERGAP Project, during two surveys carried out on 2007 on board the R/V *L'Atalante* (IFREMER). A deployment of five mini-GI airguns (Sercel®) and a three-section streamer (each one with 24 channels and 150 m long) was used during the acquisition. The location of these 2-D seismic profiles is shown on Figure 3.

3.1. Coherency Analysis of Gravity Data

As the final Bouguer anomaly grid includes both ship and satellite altimetry-derived gravity data, we have accomplished a spectral analysis of the coherence between both data sets. The aim of this analysis is to evaluate the precision and the presence of a cut-off frequency marking the accuracy lower limit of the data set derived from satellite altimetry.

For this analysis, we sampled the satellite data set along a line coincident with a long ship track, traversing the west Galicia margin (Figure 4a. See location on Figure 2). The power spectrum was calculated for both data set profiles (Figure 4c), following the procedure developed by Wessel and Smith (1995). The power values are similar for both ship and satellite profiles (Figure 4c). The coherence between both profiles has values close to 1 for the long wavelength, meanwhile for wavelengths of less than 20 km, the coherence is much lower

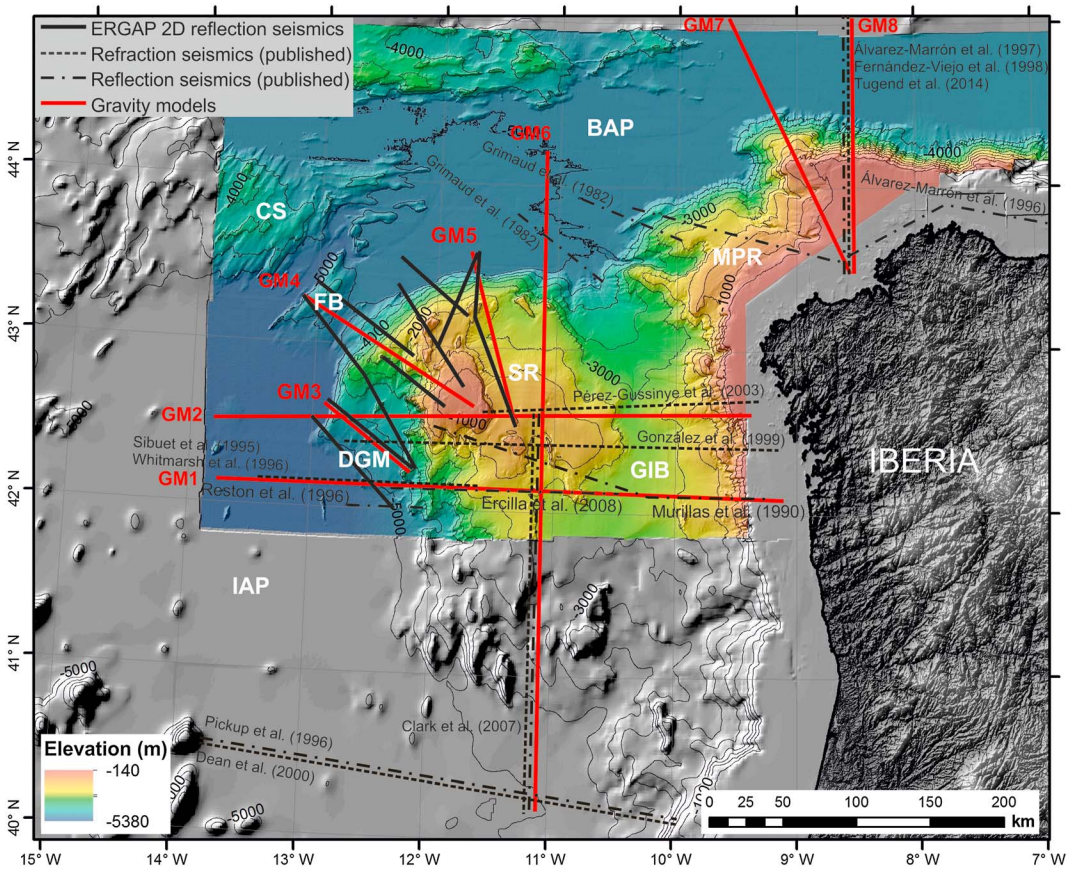

Figure 3. Digital terrain model of the study area with illumination from the NW. Contour each 500 m. Colored, swath bathymetry data set (Spanish EEZ Project), surrounded by shaded relief model from GEBCO (offshore) and SRTM (onshore). The black thick lines show the location of the original multichannel reflection seismic profiles used for this work. The dotted black lines show the location of available refraction (wide angle) seismic profiles, published by others (see reference labels). The dash-dot black lines show the location of published reflection seismic profiles (see reference labels). The red thick lines show the locations of gravity models: BAP, Biscay abyssal plain; CS, Coruña seamounts; FB, Finisterre bank; MPR, marginal platform region; SR, seamount region; DGM, deep Galicia margin; GIB, Galicia interior basin; IAP, Iberia abyssal plain.

(Figures 4c and 4d). According to these results, in areas where only satellite altimetry derived data are available, we have avoided to model blocks related to anomalies of less than 20-km wavelength.

3.2. Spectral Analysis of Gravity Data

In order to accomplish a complete gravity study, a 2-D spectral analysis of the Bouguer anomaly grid (Figure 5a) has been made, with the aim to identify linear trends characterized by different slopes that link to distinct wavelength groups (Karner & Watts, 1983), each related to different kind of lithospheric sources (Figure 6a). Afterward, frequency filtering was applied to obtain the following grids: (1) long-wavelength Bouguer anomaly grid ($\lambda > 150$ km), generally related to deep sources such as variations on the Moho topography (Figure 6b); (2) mid-wavelength Bouguer anomaly grid (150 km $> \lambda >$ 33 km) that match with gravity anomaly sources located on lower and middle crust levels (Figure 6c); and (3) short-wavelength Bouguer anomaly grid (33 km $> \lambda >$ 8 km), related to structures located on the upper crust, such as small graben and other relatively superficial anomalous bodies (Figure 6d).

3.3. Gravity Modeling

Finally, eight serially arranged 2+3/4-D density models were performed all along the Galicia margin (using Geosoft GM-SYS software), in order to analyze its across and along strike structure (Figure 3). Three of the density models are at least 360 km long, crossing the whole margin: Two are W-E oriented (GM1 and GM2), crossing from the IAP to the western Galicia continental shelf; the third one (GM6) transects the

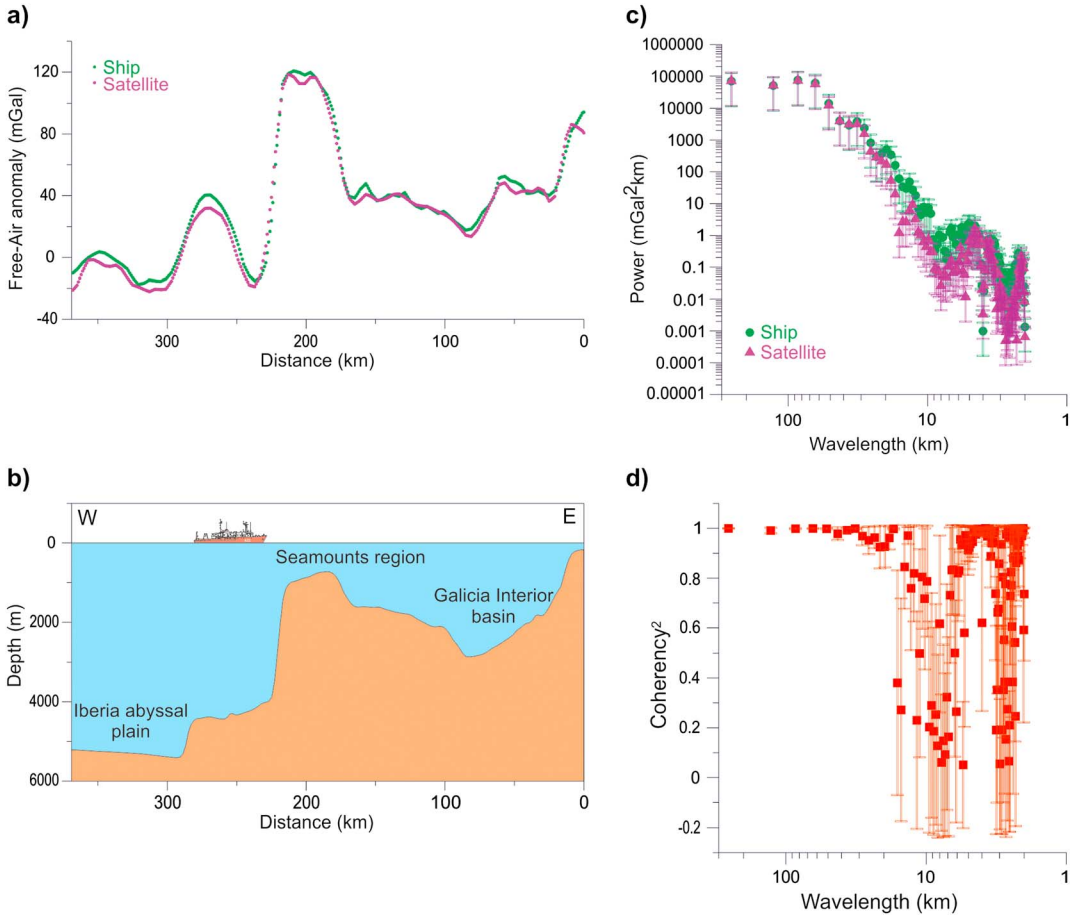

Figure 4. Coherency analysis of free-air gravity anomaly data from ship and satellite-derived data sets. Sampling interval is 1 km. See location of the sampled profile on Figure 2. (a) Ship (green) and satellite altimetry (purple) free-air anomaly values along the profile. (b) Bathymetric profile overlapping the gravity sampled profile. (c) Comparison between the ship and satellite altimetry data power spectrums calculated along the profile. (d) Coherency analysis between the ship and satellite altimetry data sets.

margin N-S from the Biscay abyssal plain (BAP), through the SR east of Galicia bank, to the IAP south of the SR and the GIB. The rest of the gravity models are shorter and serially arranged across the transition from the continental to the oceanic domain. The location of gravity models is usually conditioned by the existence of previous seismic profiles to constrain them. In our study area, most of the seismic information has been focused on the characterization of the west Iberia margin and its rift structure. As a result, the majority of the previous seismic profiles are E-W directed and located on the southern part of our interest area, and there is a lack of seismic profiling literature northwest of Galicia. Most of the gravity models constructed during this study are supported by the original seismic sections available for this study and also by previous reflection and refraction profiling carried out by others (Clark et al., 2007; Ercilla et al., 2008; Fernández-Viejo et al., 1998; González, Córdoba, & Vales, 1999; Murillas et al., 1990; Pérez-Gussinyé et al., 2003; Reston et al., 1996; Sibuet et al., 1995; Whitmarsh et al., 1996). To set Moho depth, where no refraction seismic information is available, we have used the Moho depth model constructed by Díaz and Gallart (2009), and that derived from the GOCE satellite data (GEMMA Project; Reguzzoni & Sampietro, 2015). It must be taken into account that the GEMMA model is a low-resolution global model that shows correlation errors in continental margins (Reguzzoni & Sampietro, 2015). These misfits are due to a simplistic description of the oceanic seafloor used for the model and, locally, to a lack of seismic observations (Sampietro et al., 2013). Together with the approximate Moho depth (Díaz & Gallart, 2009; Reguzzoni & Sampietro, 2015), where no coincident seismic profiles are available, we use adjacent area information by correlation of single gravity anomalies to construct models that make geological sense.

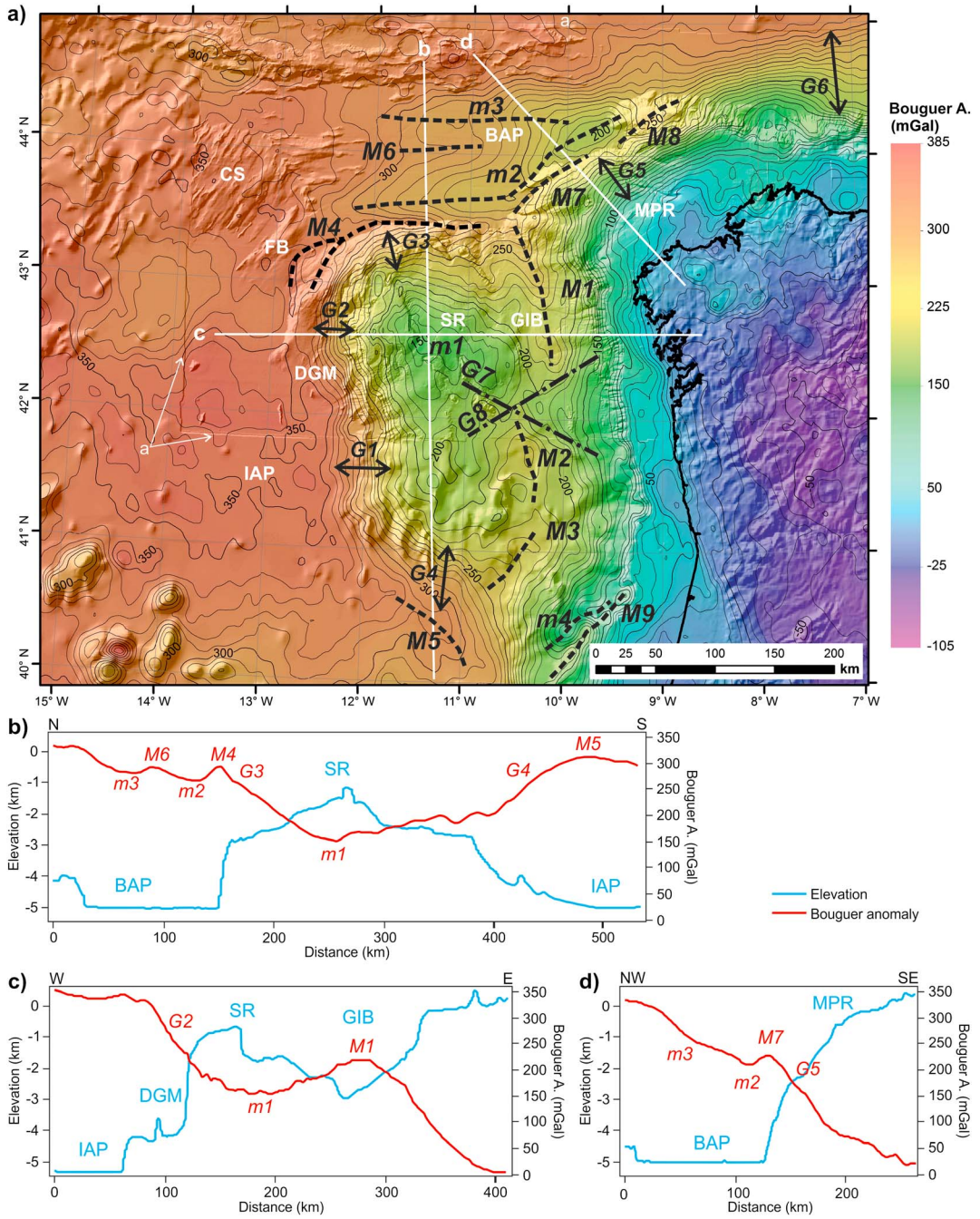

Figure 5. (a) Bouguer anomaly map (color), presented over the shaded relief model, calculated from the digital terrain model (DTM), to facilitate the connection between gravity anomalies and morphological features. The white "a" indicates artifacts on the DTM by the ship and GEBCO assemblage. Contour each 10 mGal. The dashed black lines show relative minimum (*m*) and maximum (*M*) axis. *G* indicates gradient stripes on the continent-ocean transition (black arrows) or related to strike-slip tectonic features (dash-dot black lines). (b–d) Elevation (blue) and Bouguer anomaly (red) profiles. The blue labels indicate toponymy, and the red italic labels indicate minimums, maximums, and gradients seen also on (a). BAP, Biscay abyssal plain; SR, seamount region; DGM, deep Galicia margin; GIB, Galicia interior basin; IAP, Iberia abyssal plain; MPR, marginal platform region.

This procedure has allowed modeling first-order structures that imply an important lateral density contrast, such as those of the continent-ocean transition. Modeling the first-order tectonic features along the whole Galicia continental margin complements the gravity map analysis. This allows moving forward on the

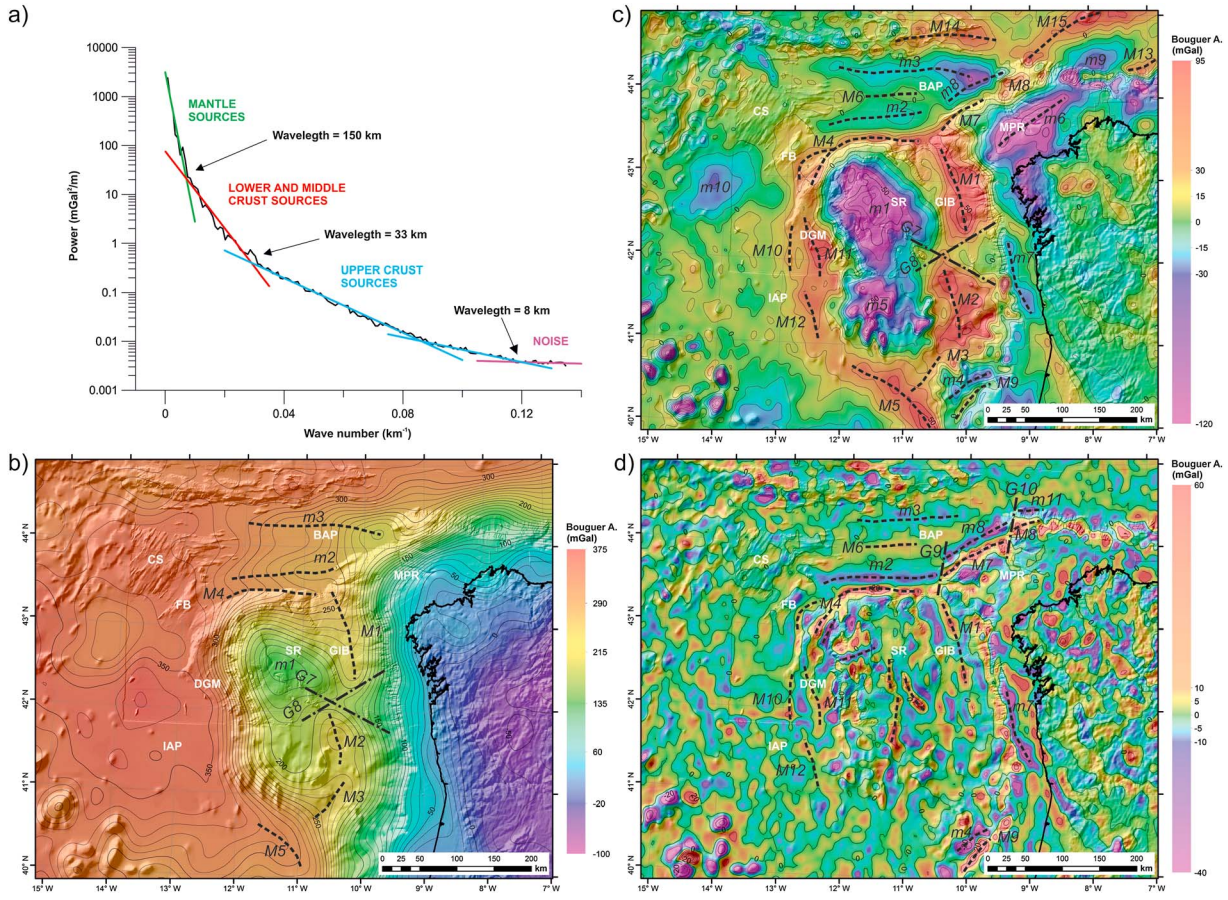

Figure 6. (a) Radial power spectrum of the complete Bouguer anomaly grid. The colored lines show the lineal approximations for every wavelength span related to each kind of gravity anomaly sources (Karner & Watts, 1983). (b) Long wavelength Bouguer anomaly map ($\lambda \geq 145$ km). Contour each 20 mGal. (c) Middle wavelength Bouguer anomaly map ($145 \geq \lambda \geq 35$ km). Contour each 10 mGal. (d) Short wavelength Bouguer anomaly grid ($35 \text{ km} > \lambda > 8$ km). Contour interval of 10 mGal. Filtered Bouguer anomaly grids are presented over the shaded relief model, to facilitate the connection between gravity anomalies and morphological features. The dashed black lines indicate Bouguer anomaly relative minimum (*m*) and maximum (*M*). The dash-dot black lines indicate gravity anomaly gradients (*G*) related to strike-slip and/or transform faults.

comprehension of the margin structure and of the transition from the west Galicia rifted margin, to the north Iberia inverted one.

Calculations of the gravity model response are based on the classic methods and algorithms (Talwani & Heirtzler, 1964; Talwani, Worzel, & Landisman, 1959; Won & Bevis, 1987). The correlation between densities and seismic wave velocities is made with the aid of the empiric relationship curves between these parameters (Barton, 1986; Brocher, 2005; Christensen & Mooney, 1995; Ludwig, Nafe, & Drake, 1970). Ten different density units are distinguished, from the refraction seismic velocities given by Córdoba, Banda, and Ansorge (1987), Sibuet et al. (1995), Whitmarsh et al. (1996), and Pérez-Gussinyé et al. (2003; Table 1). The transverse extension of the modeled blocks is prolonged perpendicularly 100 km toward each side in the case of the crustal blocks and 50 km for the sedimentary cover blocks.

4. Results and Interpretation

4.1. Bouguer Anomaly Maps

On the study area, Bouguer anomaly values vary from −105 mGal (onshore) to 385 mGal (offshore, IAP; Figure 5a). Offshore, in general terms, there is a progressive increase of the Bouguer anomaly values to the west and northward, that is, to the oceanic crust regions. On the continental basement region, Bouguer anomaly values are usually below 220 mGal, while on the oceanic regions, they are commonly over 300 mGal.

Table 1
Density Characteristics of the Units Modeled (Figures 8–11)

Unit	*P* wave velocity (km/s)	Density (g/cm^3)
Mantle	8	3.3
Serpentinized mantle	5.5–7.5	2.6–3.15
Lower oceanic crust	7.4	3.1
Upper oceanic crust	6.5	2.8
Lower continental crust	6.6	2.85
Upper continental crust	5.5	2.6
Syn-rift sediments	2.5	2.4
Postrift sediments	2	2.1

Note. Seismic velocities from Córdoba et al. (1987), Sibuet et al. (1995), Whitmarsh et al. (1996), González et al. (1999), and Pérez-Gussinyé et al. (2003). Correlation between seismic velocities and densities made with the aid of the empiric relationship curves by Ludwig, Nafe, and Drake (1970), Barton (1986), Christensen and Mooney (1995), and Brocher (2005).

West of Galicia, the SR is characterized by a striking relative minimum (*m1*, Figure 5a), roughly elongated NNW-SSE, and shifted toward the southeast from the highest elevation area (Figure 5c. See also Figure 3). It is related to the greater continental crust thickness found in the SR (e.g., Pérez-Gussinyé et al., 2003). Between this relative minimum and the 100-mGal contour to the east, which approximately matches the continental shelf break, there is a relative maximum located on the GIB (Figure 3). This maximum axis has three segments, elongated NNW-SSE (*M1* and *M2*, separated by the gradients *G7* and *G8*, on Figure 5a; see profile c) and NE-SW (*M3*, Figure 5a), according to the main structural directions. These maximums on the GIB can be attributed to the intense stretching of the continental crust during the first rifting stages (e.g., Manatschal & Bernoulli, 1999; Murillas et al., 1990). On the west margin, there are large Bouguer anomaly gradients on the transition from the continental domain (i.e., the SR) to the oceanic domain (Figure 5a): (1) West of the SR, there is an steep gradient of 3.12–3.6 mGal/km (*G1* and *G2* on Figure 5a; see profile c) elongated N-S to NNW-SSE; (2) from the northwestern flank of the SR to the BAP, there is a nearly E-W directed gradient stripe, up to 2.8 mGal/km (*G3* on Figure 5a; see profile b); and (3) south of the SR, a 2.9-mGal/km NW-SE directed gradient band connects with the IAP (*G4* on Figure 5a; see profile b). *M4* (up to 350 mGal) surrounds the SR by the north and northwest and bifurcates in the proximity of the Finisterre bank (FB); it has to be emphasized that these Bouguer anomaly values are atypical for a topographically raised area.

The transition to the oceanic domain northwest of Galicia is staggered and complex, with a 0.7 to 1-mGal/km medium gradient (G5, Figure 5a), and several relative minimum and maximum axes (e.g., *m2–m3* and *M7–M8* on Figure 5a; see profile d). The *m2* and *m3* axes seem to converge on a relative minimum of less than 200 mGal at the foot of the marginal platforms, probably related to the depocenter mapped by Grimaud et al. (1982).

North of Galicia, the transition to the oceanic domain is shown as a regular Bouguer anomaly gradient of 1.2 mGal/km (*G6*, Figure 5a).

4.1.1. Long-Wavelength Bouguer Anomaly Map

This map, related to deep anomaly sources such as variations in the Moho topography, shows a smoothed version of the great relative minimums, maximums, and gradients observed on the previous map (Figure 6b. See also Figure 5a). Thus, the great minimum on the SR (*m1*) stands out, related to a deeper Moho, and slightly displaced to the southeast from the lower bathymetry area. The maximum axis *M1–M3* on the GIB approximately coincides with the morphological axis of the basin. The relative maximum axis *M4* bordering the foot of the slope north of the SR and the relative minimum axis *m2* and *m3* on the BAP draw attention as they imply a lithospheric scale deformation, according to observations by Muñoz-Martín et al. (2010).

4.1.2. Mid-Wavelength Bouguer Anomaly Map

Here anomalies mainly related to density variations at lower and midcrustal levels are highlighted (Figure 6c). Thereby, once the regional long wave length component was removed (Figure 6b), some important anomalies are highlighted.

Among the relative maximums, the following stand out: (1) A streaking maximum axis (*M4*) bordering the SR to the NW and to the N. This anomaly stripe may be related to the presence of high density rocks, such as oceanic basement and serpentinized mantle, previously sampled on this area of the slope (Boillot, Comas et al., 1988; Malod et al., 1993; Kornprobst & Chazot, 2016); (2) west and southwestward from the SR, some relative maximum are emphasized (*M9–M11*) aligned on a wide band that narrows northward. These can be linked with the existence of high density rocks at crustal levels, such as exhumed mantle, or with an extremely thin crust, or with both effects (e.g., Dean et al., 2000; Louden & Chian, 1999; Sibuet et al., 1995; Whitmarsh & Sawyer, 1996); (3) south of the SR, the relative maximum axis *M5* is elongated NW-SE over the IAP, looking similar to *M9–M11* and in continuation with them, so it may have the same origin; (4) on the GIB, the *M1–M3* maximum axis, together with the gradient bands, *G1* and *G2* are highlighted. *M1* is slightly shifted from the morphological basin axis. These maximums are related to the continental crust thinning and consequently the rising of the lithospheric mantle along a relative narrow region (e.g., González et al., 1999; Pérez-Gussinyé et al., 2003), which lead to a mid-wavelength Bouguer anomaly; (5) *M7–M8* are

located at the foot of the marginal platforms and can be considered as a prolongation of *M4*. They may be related again with the elevation of oceanic crust and the presence of a narrow stripe of serpentinized mantle, incorporated into the morphological continental slope; (6) on the BAP, *M13* and *M14* axes are elongated coherent with main structural directions and may be linked with a thicker oceanic crust, possibly also related to a slight compressional deformation (Medialdea et al., 2009).

From the relative minimums observed in this mid-wavelength map, we note (1) the great minimum *m1* located over Galicia bank (the most prominent high on the SR) and other surrounding structural highs. Southward, this relative minimum area continues with *m4*, centered on other structural highs. These minimums may be related to the relative thicker continental crust and an important sediment cover (e.g., Montadert et al., 1974; Wilson et al., 1989); (2) facing the northwestern shore of Galicia, *m5* axis, NE-SW directed, is located on the MPR. These marginal platforms are former graben basins, with important sediment thickness (up to 3 s TWTT), tectonically inverted and uplifted during the Pyrenean orogeny (Murillas et al., 1990); (3) the relative minimum axis *m6*, elongated NNW-SSE, is found over the Porto basin on the continental shelf (Murillas et al., 1990); (4) NW and N of Galicia, *m7* and *m8* are located at the foot of the compressional belt. Their location and relation with surrounding maximums indicate that they could be linked with the existence of important sediment depocenters ahead of the compressional front, as previously shown by Grimaud et al. (1982); (5) south of the Coruña seamounts (Figure 1), within the IAP, another large minimum is found (*m9*), also noticeable on the Bouguer and long wavelength Bouguer anomaly maps, although less striking there. This last minimum is probably related to another sedimentary depocenter, which would be the distal part of the Biscay turbidite systems (Jané et al., 2011).

4.1.3. Short-Wavelength Bouguer Anomaly Map

On this map, we notice the maximum axis bordering the continental margin, close to the foot of the slope, to the NW and N of the SR (*M4*), following to the N of the GIB and at the foot of the MPR (*M7*), and to the northern margin (*M8*). Together with, and parallel to these maximum axis, three separate minimum axes are also observed to the north (*m2*, *m7*, and *m10*). This minimum-maximum axis belt seems to be related to the compressional front and the elevation of oceanic crust there (relative maximums), with probably associated basins in the foreland (relative minimums). The continuity of this anomaly belt is interrupted by means of NNE-SSW trending gradients *G9* and *G10* (see Figure S1 in the supporting information). The orientation of these gradients is coherent with the main lineament orientations observed by Maestro et al. (2017) on this region north and northwest of Galicia, from a detailed bathymetry analysis. The NNE-SSW structural direction is observed also on land (e.g., Guimaraes-Orense-Eo, Regua-Verín, and Manteigas-Vilariça-Bragança strike-slip fault systems. See Figure 1; e.g., De Vicente, 2004; De Vicente et al., 2008; De Vicente & Vegas, 2009; Rockwell et al., 2009; Tavani, 2012) and elsewhere offshore in the north Iberia margin for first-order strike-slip and transfer faults (e.g., Roca et al., 2011) connecting different segments of the Late Jurassic-Early Cretaceous rift system (Tugend et al., 2014, and references therein).

4.2. Seismic Profiling and Gravity Modeling: Combined Interpretation

Here we present the selection of the gravity models and, where available, coincident or nearby original seismic profile interpretation. The different sections are described following a clockwise direction, covering the whole northwest Iberia margin from west to north Galicia.

As shown below, for the sake of geological consistency with adjacent interpretations and in the absence of sampling or seismic evidence, in models GM5–GM7, we have opted to model a serpentinized mantle unit, somewhat underthrusted in the transition from the continental to the oceanic domains. This is possible because the densities of the serpentinized bodies are variable (from 2.4 to 3.3 g/cm^3) and in the range of the continental and oceanic basements. A more conservative model construction, without considering the existence of this unit, can be also achieved without outstanding differences in the overall shape of the model. In fact, on the gravity model GM8 (Figure 11), coincident with the IAM-12 seismic line (Fernández-Viejo et al., 1998; Tugend et al., 2014), a serpentinized mantle unit can be included at the base of the continental crust, according to the interpretations by Tugend et al. (2014), although Fernández-Viejo et al. (1998) did not make this distinction on their seismic and gravity models.

4.2.1. GM1 Model

The gravity model GM1 crosses the main Early Cretaceous rift structures of west Galicia margin, south of the SR, in a region without remarkable tectonic inversion features (Figure 7). It is supported by refraction seismic

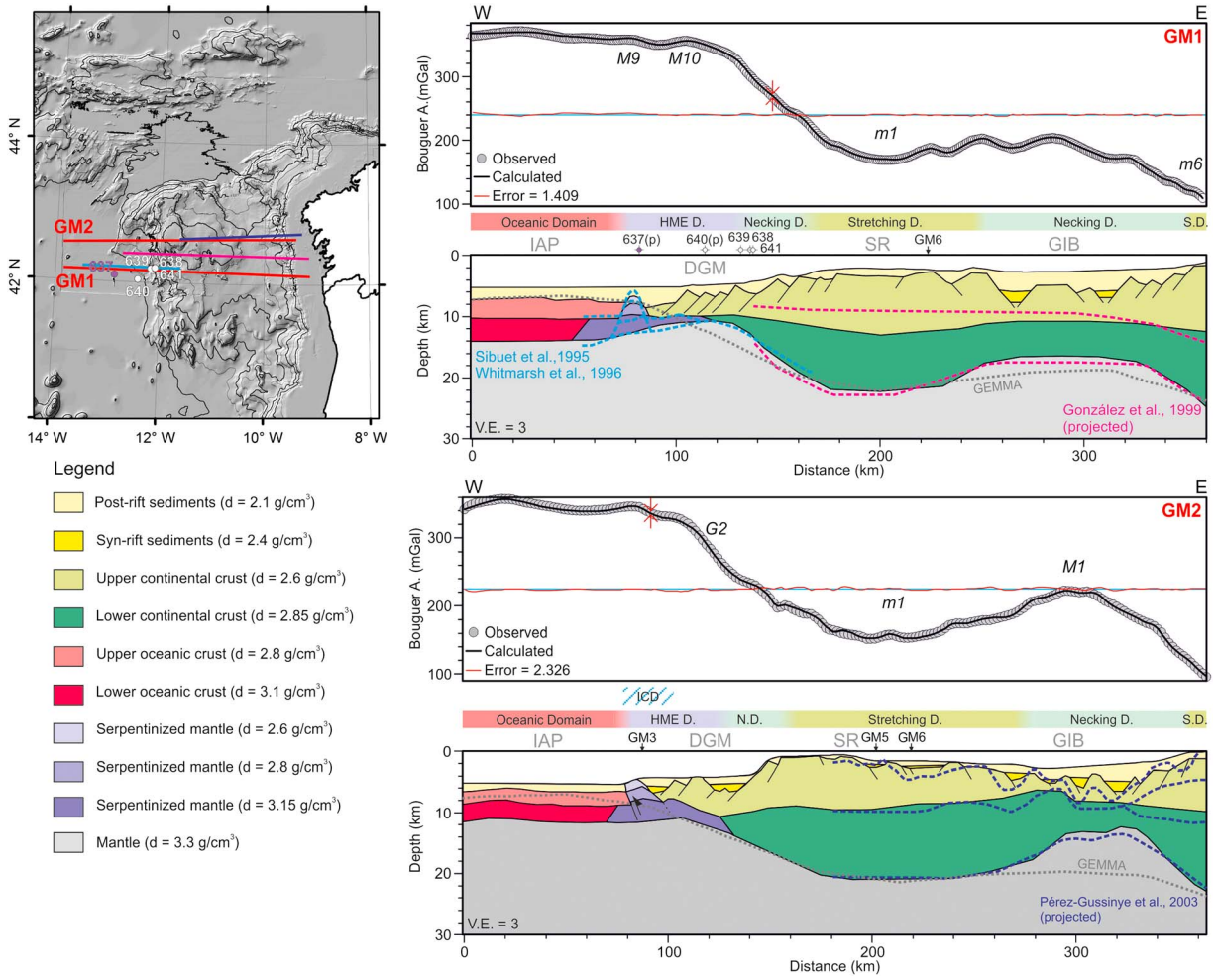

Figure 7. Gravity models GM1 and GM2, crossing the western margin. The italic labels on the Bouguer anomaly curves indicate relative maximums (*M*), minimums (*m*), and gradients (*G*) also labeled on the Bouguer anomaly map (Figure 5a). Some horizons from published refraction seismic models are plotted (and referenced) over the gravity models (dashed colored lines; see location on the map and on Figure 3). GEMMA Moho depth model profiles are also plotted on the gravity models (dashed gray line). ODP leg 103 drill hole locations are plotted on the insert and along GM1, p: location projected.

data on its western side (González et al., 1999; Sibuet et al., 1995; Whitmarsh et al., 1996), and by reflection seismic profiles interpreted by Murillas et al. (1990), Reston et al. (1996), and Ercilla et al. (2008). The proposed model shows a great stretching in the GIB, where a thick sediment sequence can be found (>5 km). To adjust the relative maximum at the GIB (see *M1–M2*, Figure 5a), the Moho is modeled to be located at a minimum depth of 16 km, rising symmetrically. At the SR, the Moho is modeled at a depth up to 22 km, soaring westward on the DGM zone. Here the continental crust is extremely stretched, and its lower unit is delaminated until it retreated at the distance of 118 km. From this point to the 68-km distance, a high density unit of serpentinized mantle is modeled, rising westward as a ridge, and with some upper continental crustal blocks resting on it. The serpentinized mantle unit prolongs ~20 km westward from the distal ridge, underlining an anomalously thin oceanic basement (Davy et al., 2016; Sibuet et al., 1995). Along the DGM zone, Bouguer anomaly values are higher and stable, in the range of those typical of an oceanic crust, so the previous seismic information is essential to constrain the modeling. It should be noted that there is a striking difference between the global Moho depth model (Reguzzoni & Sampietro, 2015) and the refraction seismic constraints along the DGM and the IAP.

4.2.2. GM2 Model

The gravity model GM2 is approximately parallel to the previous one, traced northward, and crosses the southwest edge of the compressional front (Figure 7). It is supported by wide-angle and reflection seismic

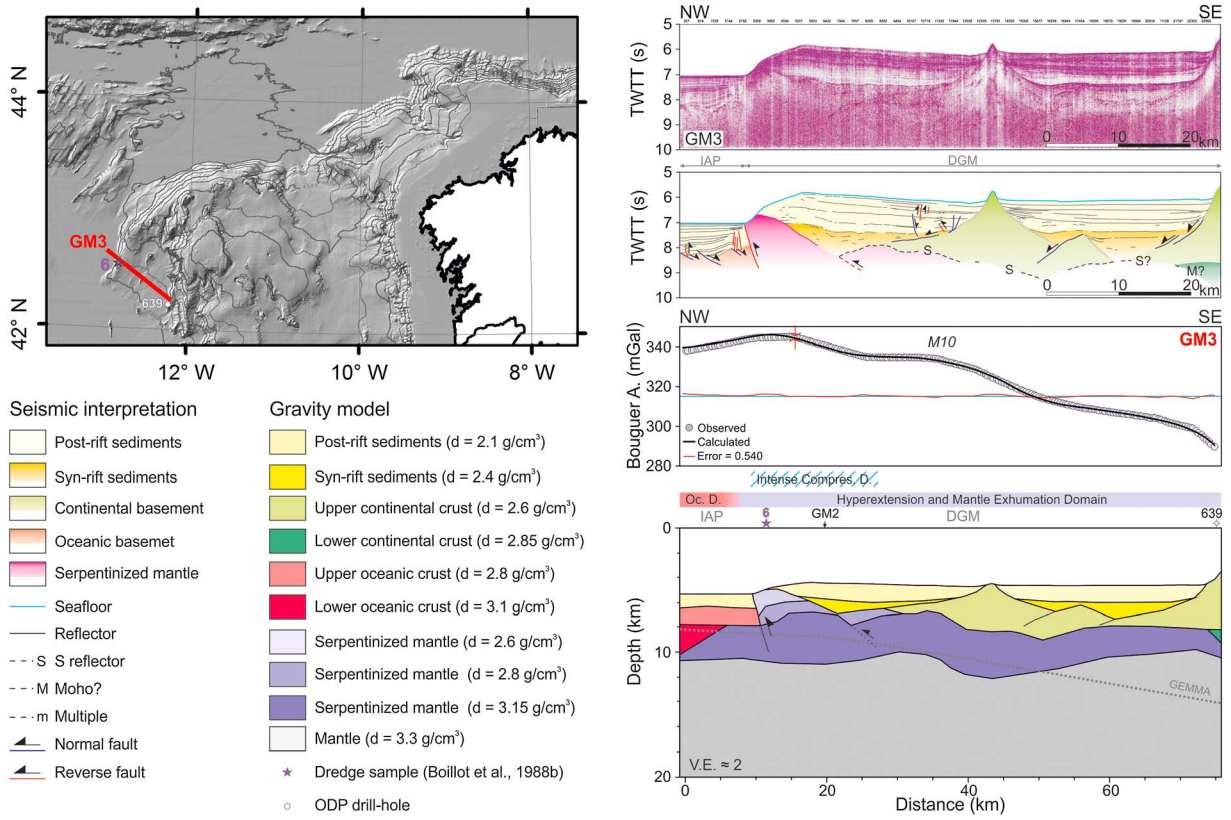

Figure 8. Coincident seismic profile and gravity model GM3. The seismic profile is shown with its line-drawing interpretation below. Dredge sample by Boillot, Comas et al. (1988) and ODP leg 103 drill hole (white circle) are located on insert and on the interpreted seismic profile (purple star). GEMMA Moho depth model profile is plotted on the gravity model (dashed gray line).

data from Pérez-Gussinyé et al. (2003) and reflection seismic profiles from Murillas et al. (1990) and Ercilla et al. (2008). To adjust the relative maximum *M1* on the Bouguer anomaly curve (Figure 7; see also Figures 5a and 6b and 6c), it is necessary to model a Moho rising under the stretched continental crust of the GIB. The Moho is modeled there at a minimum depth of 12 km, according to the observations of Pérez-Gussinyé et al. (2003). Also, on the GIB, the section shows depocenters of up to 5 km thickness (Pérez-Gussinyé et al., 2003). This Moho rising is narrower than that observed on de model GM1, asymmetric, and slightly shifted from the morphological basin axis. At the SR, the Moho is at a maximum 21 km depth (related to *m1*), and eastward offset from the bathymetric minimum (Galicia bank). To the west, continental crust stretching and Moho soaring occur in a narrower band, from 85 to 138 km distance, related to a steeper Bouguer anomaly gradient (*G2*, Figures 5 and 7). As in GM1, the lower continental crust is delaminated up to disappear, and a serpentinized mantle unit is modeled at the DGM, underlining upper continental crustal blocks (85 to 112 km distance). The serpentinized mantle unit forms a distal ridge, outcropping at the seafloor, and prolongs oceanward ~15 km below the first thin oceanic basement. This ridge is modeled overthrusting the oceanic crust basement, according to the compressional structures observed previously in this area (e.g., Boillot et al., 1995; Grimaud et al., 1982; Groupe Galice, 1979; Vázquez et al., 2008), and in agreement with the seismic interpretation and modeling along profile GM3 (see below), which crosses the compressional front slightly northward of this model (Figure 8). To adjust the model with the Bouguer anomaly curve, it is necessary to model a convex morphology of the serpentinized mantle unit east of the ridge; this morphology could be also related to the compressional deformation.

4.2.3. GM3 Model

The seismic and gravity section GM3 (Figure 8) is representative for the structure of the transition to the oceanic domain in the DGM. This profile, NW-SE directed, crosses the southwest end of the compressional front from the IAP to the DGM, southeast of the Galicia bank. Thus, this section traverses the main

compressional features but is oblique to the main rifting structures. On the seismic section, three different types of acoustic basements can be identified (continental, oceanic, and serpentinized mantle). To the southeast, the *S* reflector is interpreted as a group of bright reflectors, with relative continuity, underlining the continental crust basement (Reston et al., 1996). This continental basement seems to be extremely thinned, with faulted and tilted blocks, locally isolated. Below these tilted continental basement blocks, and with the *S* reflector at the top, the serpentinized mantle basement is interpreted. Northwestward, this unit rises with a ridge shape, which outcrops at the foot of the slope (Boillot, Comas et al., 1988). To the northwest, the sedimentary cover is intensely deformed over the oceanic crust basement close to the serpentinized crust ridge. The contact between this serpentinized mantle ridge and the oceanic crust to the northwest is interpreted as a reverse fault, with a 0.8-s (TWTT) dip-slip throw. On the continental domain, a syn-rift sedimentary sequence is identified, locally overlaying the serpentinized mantle unit, and the post-rift sedimentary sequence is only slightly deformed. On the coincident gravity model, we use the GEMMA Moho depth model (Reguzzoni & Sampietro, 2015) as an initial approximation, although on the final forward modeling, Moho depth moves away from this global reference. This difference is also observed at the nearby GM1 model in the DGM. In order to adjust the architecture of the basement top interpreted from the coincident reflection seismic profile, it is necessary to model a wide high density unit, which corresponds to the serpentinized mantle body, sampled nearby by Boillot, Comas et al. (1988). This unit has a distal ridge outcropping at the foot of the slope, related to the Bouguer anomaly maximum observed on this profile (at 13 km distance). Again, we have modeled a compressional feature at the contact between this ridge and the adjacent oceanic crust and a small bulge of the serpentinized mantle unit (at 28 km distance), probably related also to a thrust. The serpentinized mantle unit prolongs more than 10 km oceanward from the distal ridge, below a thin oceanic crust similar to that observed by Davy et al. (2016) further south.

4.2.4. GM4 Model

The next section to the northwest corresponds to gravity model GM4 and the nearby seismic profiles GM4a and GM4b (Figure 9). Seismic line GM4a is NW-SE directed, crossing the FB, and the lower continental slope, transecting the compressional front to the northwest of the SR (Figure 9). According to the observations done over the Bouguer anomaly map (Figure 5), most of the basement along the seismic profile is interpreted to be oceanic, faulted and tilted to the northwest, with FB acting as a sediment trap. In the compressional front, an oceanic basement thrust with a dip-slip throw of about 1.2 s (TWTT) is identified, making the oceanic basement outcrop at the foot of the continental slope. Southwest of this oceanic basement thrust, we interpret a thrust at the base of the serpentinized mantle ridge, making its outcrop at the continental slope (according to nearby dredge samples by Boillot, Comas et al., 1988; see also Figure 1), with a large morphologic escarpment. The sedimentary cover on the oceanic crust is thick (about 1.7 s, TWTT), showing a moderate-to-intense compressional deformation. Seismic line GM4b (Figure 9) is also NW-SE directed. It crosses from the proximal part of the northwestern flank of the SR, to the top of Galicia bank. Here the whole acoustic basement is interpreted as continental in origin (see Bouguer anomaly map, Figure 5) and is faulted and tilted to the northwest. The sedimentary cover thickness is variable, reaching at least 2 s (TWTT) northwest of the García structural high, where some compressional deformation can be interpreted. The nearby GM4 gravity model transects part of the oceanic fabric reliefs (FB) and the compressional front, finishing at Galicia bank (SR; see location on Figures 3 and 9). On its northwestern side, it coincides with the GM4a seismic profile, and the proximal half of the model is nearly parallel to GM4b seismic profile (8 km to the southwest). To construct this gravity model, we use the GEMMA Moho depth model (Reguzzoni & Sampietro, 2015) as a first approximation for this surface, although some discrepancies arise between the global model and the final GM4 model. The basement type and the overall basement top architecture interpreted on the nearby seismic profiles GM4a and GM4b are extrapolated on GM4. In this case, the transition from the continental Bouguer anomaly values to those regular values of the oceanic domain is narrower, with the exhumed mantle unit outcropping at the foot of the slope (sampled by Boillot, Comas et al., 1988). Differing from the previous models, the hyperextension and mantle exhumation (HME) domain is narrower. Here the upper continental crust seems to be moderately thickened close to the transition to the oceanic domain (consistent with the compressional deformation observed on the seismic section GM4b) and is modeled with a relatively constant thickness along the whole model. To fit with the Bouguer anomaly values, a relatively thin lower continental crust density unit is modeled next to the serpentinized mantle body, and the upper continental crust unit is modeled with a relatively constant thickness of 6 km. A 3-km depocenter is modeled close to the serpentinized mantle

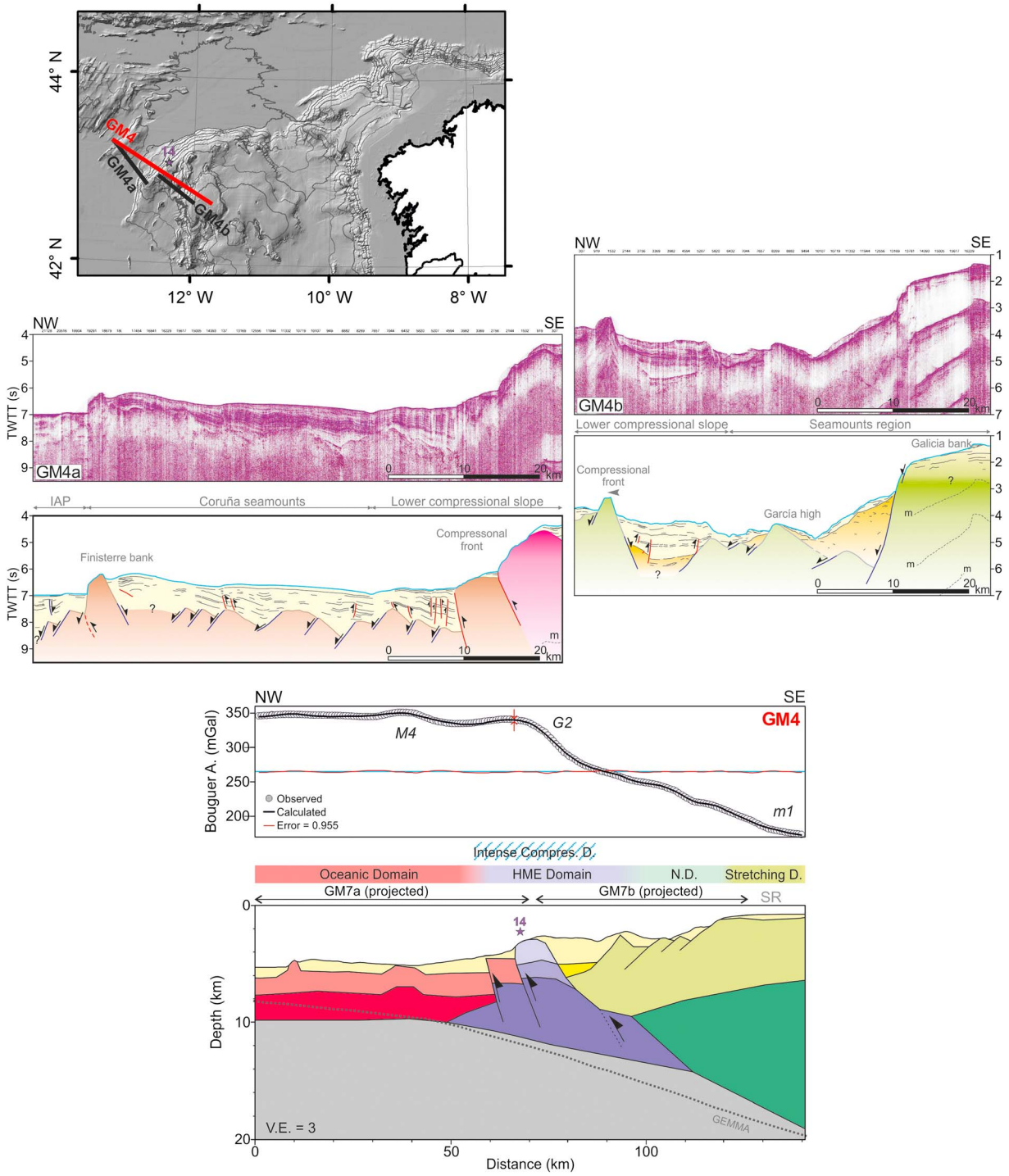

Figure 9. Seismic profiles GM4a and GM4b with their line-drawing interpretations below and the nearby GM4 gravity model. In the location map, both the seismic profiles (black lines) and the gravity model (red line) are shown. See legend for seismic interpretation and gravity model on Figure 8. Dredge sample by Boillot, Comas et al. (1988) located on the insert and on the interpreted seismic profile (purple star). GEMMA Moho depth model profile is plotted on the gravity model (dashed gray line). The italic labels on the Bouguer anomaly curve indicate relative maximum *M4* and gradient *G2* also labeled on the Bouguer anomaly map (Figure 5a).

ridge to adjust the relative Bouguer anomaly inflection (relative minimum at 87 km distance) in the gradient, similar to the depocenter observed on the seismic profile GM4b. A reverse structure, uplifting the oceanic basement unit, is modeled to accommodate the small relative maximum at 63 km distance, consistent with the oceanic basement thrust observed on the GM4a seismic profile.

4.2.5. GM5 Model

Northward, the next section crosses from the BAP to the north of the SR, spanning the compressional lower slope and the Ordoño structural high, following on the SR parallel to the eastern slope of Galicia bank (7 km away, see Figure 10). Seismic lines GM5a and GM5b are interpreted together, as they are continuation from each other, and close to them, the gravity section GM5 is modeled (Figure 10). Basaltic oceanic seafloor dredge samples were recovered at the foot of the slope in the vicinity of this profile (Boillot, Comas et al., 1988). As there is no additional information to distinguish a serpentinized mantle basement, on the seismic profile, only oceanic and continental basement types are interpreted. The continental basement is interpreted on most of the composed seismic section, affected by normal faulting, although the basement top is not easily identified along the southern half of the profile. No first-order tectonic features are observed on the southern half of the section because it is parallel to the main structural direction in this region. To the north, the continental basement outcrops on the Ordoño structural high, limited by normal faults, and also at the lower slope. The contact between the continental and the oceanic basements is made by means of a reverse fault that places a continental basement block over the oceanic basement, resulting on a morphological escarpment at the continental slope. A proximal oceanic basement block overthrust is interpreted to the north on the compressional front (vertical displacement of about 0.5 s, TWTT), outcropping at the foot of the slope. The sedimentary cover is slightly deformed close to the compressional front, and no compressional deformation is observed on the sedimentary cover of the continental crust south of the Ordoño high. To construct the gravity model GM5, the GEMMA Moho depth model (Reguzzoni & Sampietro, 2015) is used, and the nearby composed seismic profile is used to approximately constrain the basement top morphology. A serpentinized mantle unit can be postulated in the transition between the oceanic and the continental basement units, as an underthrusted body at the base of the compressional belt (similar to that interpreted north of Galicia by Tugend et al., 2014). The modeled continental crust thickness is fairly constant (about 14–18 km), from 60 km distance to the SSE edge of the model. From 60 to 25 km distance, the continental crustal thinning is modeled as a thinning of the lower crust unit, underlined by the serpentinized mantle unit. The transition from the continental to the oceanic domain consists of a first-order thrust. To adjust the Bouguer anomaly maximum at 16 km distance (*M4* on Figures 5a and 10), an oceanic crust thickening is modeled, by means of another thrust that makes the oceanic basement outcrop at the foot of the slope, according to the GM5a seismic profile interpretation (Figure 10).

4.2.6. GM6 Model

The GM6 gravity model (Figure 11) starts on the BAP, transects the SR east of Galicia bank, and finishes on the IAP. From the southern part of the SR to the south edge, this model is nearly coincident with the reflection and refraction seismic profile ISE-9 (Clark et al., 2007). Apart from the mentioned refraction model, the GEMMA Moho depth model (Reguzzoni & Sampietro, 2015) is used as an approximation in the northern half of the section. The modeled continental crust shows significant differences north and south of 240 km distance. Northward, the thickness of the upper and lower levels is similar. Southward, to keep the Moho depth given by Clark et al. (2007), it is necessary to model a relatively thicker lower continental crust unit to adjust the observed Bouguer anomaly. On the southern half of the model, the steeped gravity gradient is related to thickenings of the lower continental crust unit, and upper continental crust blocks, probably faulted and tilted to the south. Southward from 340 km distance, lower continental crust is thinned until it disappears (at 370 km distance, *G4*. See also Figure 5a). The upper continental crust is also extremely thinned, and the whole crustal thickness is less than 10 km. Southward, on the IAP, it is necessary to model an anomalous, high density basement, with its base at a depth of 14 km. This basement could be similar to that modeled at the DGM (models GM1, GM2, and GM3; Figures 7 and 8), probably composed of serpentinized mantle, and is consistent with the observations made on the traverse seismic reflection and refraction profile (Pickup et al., 1996; Dean et al., 2000) that is crossed by this model on its southern edge (Figure 3). On the northern half of the model, the regular Bouguer anomaly gradient is related to a thinning structure similar to that modeled at the GM5 model: thinning of the lower continental crust unit and a thrust of the continental crust over the oceanic one, with an underthrusted serpentinized mantle unit. The relative Bouguer anomaly maximum at 87 km distance (*M4*), close to the continent-ocean transition, is related to oceanic basement overthrust (see Figures 5a and 6c and 6d). This oceanic basement thrust is modeled involving a flexure of the footwall, with an associated depocenter, that accommodates the relative mid-wavelength minimum on the Bouguer anomaly curve (*m2* on Figures 5, 6, and 11).

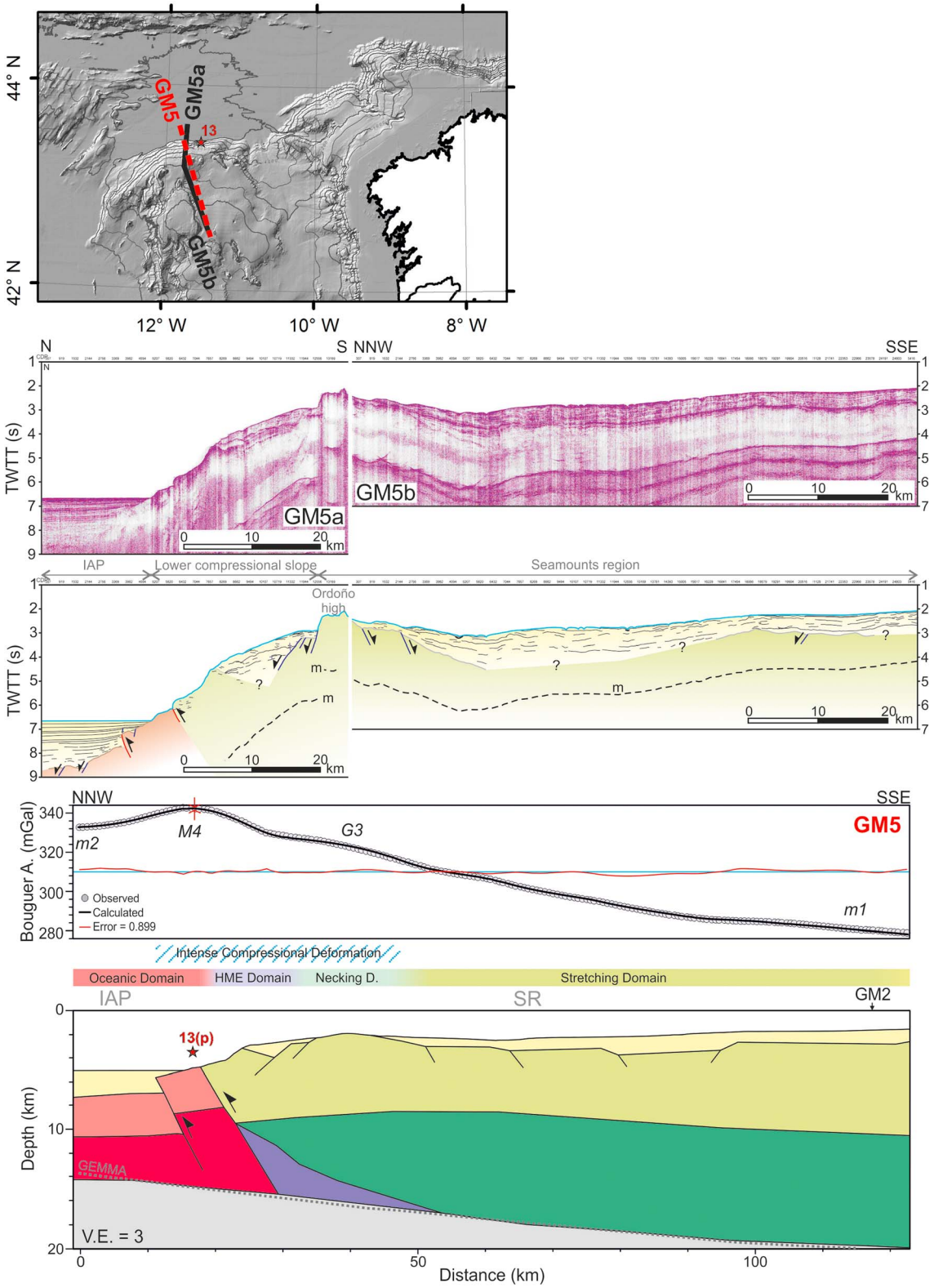

Figure 10. Seismic profiles GM5a and GM5b with their line-drawing interpretations below and the nearly coincident gravity model GM5. In the location map, both the seismic profiles (black lines) and the gravity model (red dashed line) are shown. See legend for seismic interpretation and gravity model on Figure 8. Dredge sample by Boillot, Comas et al. (1988) located on the insert and on the interpreted seismic profile (red star). GEMMA Moho depth model profile is plotted on the gravity model (dashed gray line). The italic labels on the Bouguer anomaly curve indicate relative maximum *M4*, gradient *G3*, and relative minimum *m1* also labeled on the Bouguer anomaly map (Figure 5a).

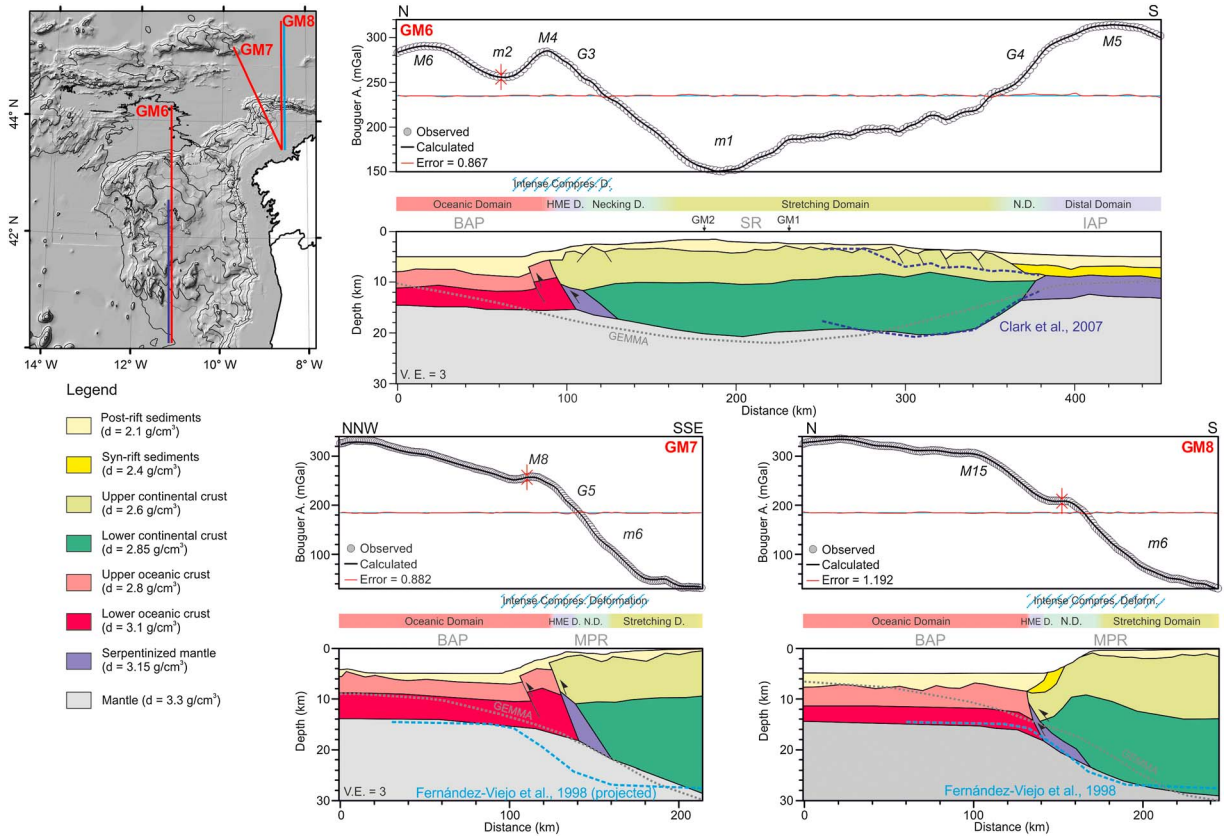

Figure 11. Gravity models GM6 (north-south directed, crossing the whole margin from the Biscay abyssal plain to the southern Iberia abyssal plain), GM7, and GM8 (northwest of Galicia). The italic labels on the Bouguer anomaly curves indicate relative maximums (*M*), minimums (*m*), and gradients (*G*) also labeled on the Bouguer anomaly map (Figure 5a). Some horizons from published refraction seismic models are plotted (and referenced) over the gravity models (dashed colored lines; see location on the map and on Figure 3). GEMMA Moho depth model profiles are also plotted on the gravity models (dashed gray line).

4.2.7. GM7 Model

The gravity model GM4 is NNW-SSE directed. It starts on the BAP, crosses the MPR on their northeast sector, and finishes on the continental shelf (Figure 11). As an approximation to Moho depth modeling, we have used both the global GEMMA model (Reguzzoni & Sampietro, 2015), mainly used to constrain the continental and transition areas, and a projection of the Moho modeled from the nearby IAM-12 refraction profile (Fernández-Viejo et al., 1998), particularly to constrain Moho depth on the oceanic domain. The smooth Bouguer anomaly gradient over the BAP is adjusted in the model as a progressive deepening of the oceanic crust basement. The relative Bouguer anomaly minimum-maximum association (at 100 and 115 km distance, respectively) is solved, as previously on the GM6 model, by means of an oceanic basement overthrust (*M8* on Figures 5 and 7) uplifting the oceanic basement in the continental lower slope, and a small foredeep-type basin (see Figure S2). The oceanic basement overthrust would have a morphological imprint as a relief at the foot of the slope. The transition to the continental domain is noticeable on the Bouguer anomaly profile as a clear inflection of the curve, with a steeper gradient on the continental domain. This transition is modeled as a reverse feature, with an underthrusted serpentinized mantle unit, similar to the one interpreted on the nearby IAM-12 seismic profile (Tugend et al., 2014). The upper continental crust unit has a nearly constant thickness; meanwhile, the lower continental crust thins oceanward. The short wavelength relative minimums on the continental domain are modeled as local depocenters originated during the extensional stage on this margin sector and partially inverted under the compressional regime (Murillas et al., 1990).

4.2.8. GM8 Model

The GM8 gravity model is N-S oriented, starting at the BAP, crossing the compressional front north of Galicia, and finishing on the continental shelf at the same point as the GM7 model (Figure 11). It is coincident with the seismic model IAM-12 (see Figure 3; Fernández-Viejo et al., 1998). Moho depth is modeled from the IAM-12 results (Fernández-Viejo et al., 1998), which differs from the GEMMA Moho depth model (Reguzzoni &

Sampietro, 2015; Figure 11). The main Bouguer anomaly gradients are fitted in the model by the Moho southward deepening. At the continent-ocean transition, the relative maximum amplitude (at 157 km distance) is lower than that observed on the previous model profiles. Thereby, and according to the previous works (Álvarez-Marrón et al., 1997; Fernández-Viejo et al., 1998), it is not necessary to model an oceanic basement thickening, and the continental domain reaches the foot of the slope. To adjust the mid-wavelength minimum located at 144 km distance, it is necessary to model a 2.3-g/cm^3 density block at the foot of the slope, which can be related to the accretionary sedimentary wedge (Tugend et al., 2014), which is coherent with the seismic velocity observed there by Fernández-Viejo et al. (1998). To fit the mid-wavelength relative maximum at 160 km distance, a high density block is modeled at the base of the continental crust, which could correspond to an underthrusted serpentinized mantle relict (Tugend et al., 2014).

4.3. Structural Domain Mapping

As explained before (section 1.1), geometrical and structural-based domain partitioning of rifted margins has been suggested (Péron-Pinvidic et al., 2013; Sutra et al., 2013; Tugend, Manatschal, & Kusznir, 2015). An approximation from both gravity and magnetic signatures has been recently made by Stanton et al. (2016) for the Iberia-Newfoundland conjugate margins at a regional scale.

The detailed gravity analysis that we have achieved allows an initial approach to the continental and oceanic domain mapping along the margin. Distinct morphostructural features observed along the margin are associated to different deformation processes. Moreover, these deformation processes may leave an imprint on the Bouguer anomaly signal. Except for the intense compressional deformation domain, most of the structural domains described here are rift-related (described above on section 1.1). The boundaries between these domains are usually diffuse, and the intense compressional deformation domain overlaps the others.

Here we propose additional criteria for a detailed characterization of rift domains along the Galicia margin (Figure 12), based on gravity data analysis and modeling. To accomplish this continuous mapping, we first identify each domain on the gravity (seismic-supported) models. Subsequently, gravity maps allow an extrapolation to complete the domain mapping gaps between models.

4.3.1. Rift Domains

4.3.1.1. Stretched Domain

This domain is mapped bordering the continental shelf to the west margin and northwest of Galicia (MPR) and on the SR (Figure 12). In this domain, crustal thinning is moderate, and faulting of the upper crust generates small graben and half-graben basins. Bouguer anomaly values are intermediate, from 90 to about 200 mGal (Figure 5a). The SR is mapped as *stretched domain* because, although crustal thickness here is less than 30 km, basement top and Moho surfaces are approximately parallel, and the characteristic wedge shape of the crust of a necking domain is not observed (Péron-Pinvidic et al., 2013). The Moho is found at a depth between $>$22 km in the continental shelf region, and 18–21 km in the SR, where the staged rift evolution left this continental ribbon (Naliboff et al., 2017; see Figures 7 and 9–11).

4.3.1.2. Necking Domain

On the study area, crustal thickness in the necking domain usually decreases from 22 km or less than 10 km, then there is a Moho inflection and it rises, tending to converge with a deepening continental basement top. Unlike the domain mapping made by others (e.g., Chenin et al., 2015; Tugend et al., 2014), considering a crustal thickness between ~30 and 10-km criterion, the primary use of the specific wedge shape of the crust approach, with converging Moho and basement top surfaces (Péron-Pinvidic et al., 2013), allows us to distinguish two main necking regions on the west Galicia margin. These are as follows:

1. The necking domain of the GIB, where intense thinning can be associated to the first rifting episode (Berriasian-Valanginian; Murillas et al., 1990). Here Moho rises from 22–18 km to 12 km depth (Pérez-Gussinyé et al., 2003; Figure 7), and this ascent is associated to a positive mid-wavelength Bouguer anomaly (Figure 6c). Locally, crustal thickness is slightly below 10 km thick (GM2, Figure 7), and it is possible that embrittlement of the whole crust could have been reached. As no fault penetration is observed in the mantle at that point (Pérez-Gussinyé et al., 2003), the westward jump of the rift axis should have occurred just before the onset of hyperextension in the GIB.
2. The necking domain westward of the SR, where the intense crustal thinning is related to the final rifting stage (Hauterivian-Aptian; Murillas et al., 1990). Here there is a correlation between this domain

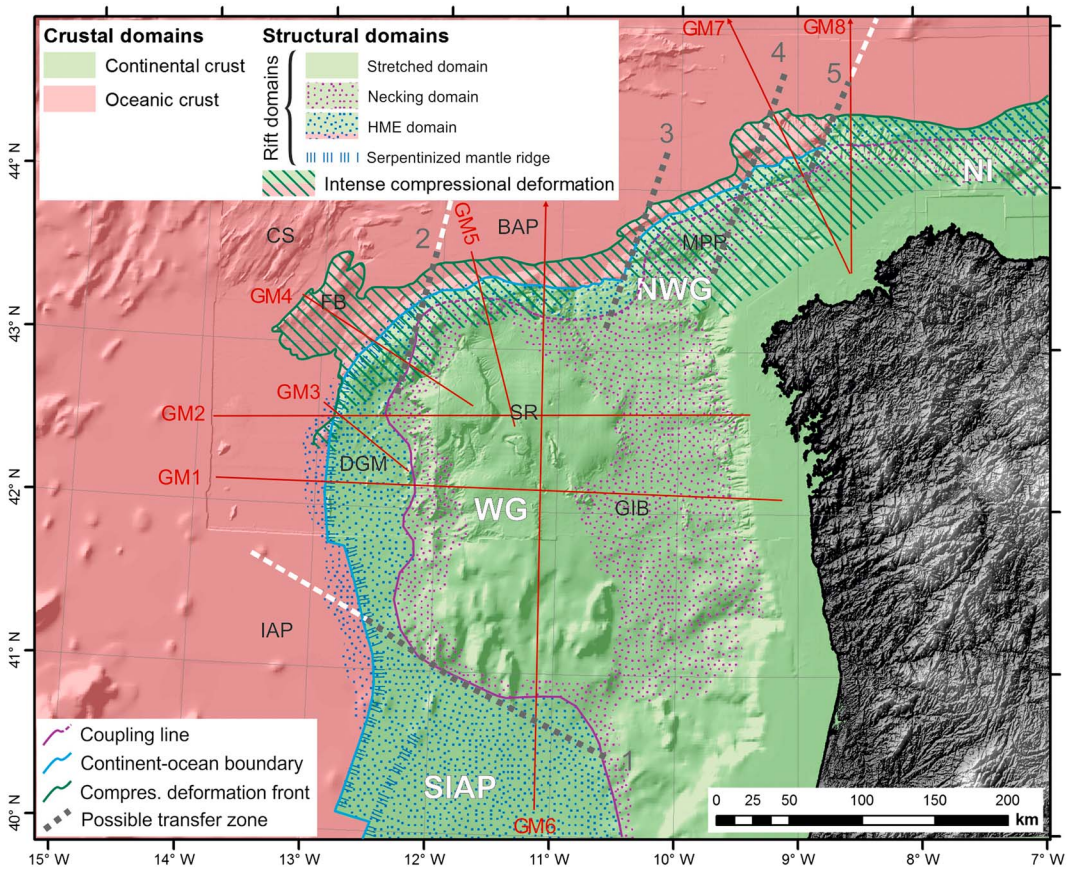

Figure 12. Crustal and structural domain map (color), over shaded relief map from the DTM. CS, Coruña seamounts; BAP, Biscay abyssal plain; MPR, marginal platform region; FB, Finisterre bank, SR, seamount region; DGM, deep Galicia margin; GIB, Galicia interior basin; IAP, Iberia abyssal plain. The coupling line indicates the border between coupled and decoupled crustal deformation. COB is interpreted from all the available data, including gravity, seismic, bathymetric, and sampling information (see Figures 1–6). The deformation front is the distal border of the area where intense compressional deformation is interpreted. The possible transfer zones are areas where gravity data, and also morphology, indicate the existence of lineal features that could play as transfer zones during rifting. The dashed white lines indicate approximate limits between the different segments of the margin: SIAP, south Iberia abyssal plain segment; WG, west Galicia segment; NWG, northwest Galicia segment; NI, north Iberia segment.

and the Bouguer anomaly gradient (see *G1*, *G2*, and *G4* on Figure 5a), similar to that observed by Stanton et al. (2016).

North of the SR and northwest of Galicia, the compressional deformation overprint avoids an accurate identification of the distal boundary of this domain, and we are not able to identify the points of 10-km crustal thickness in the former rifted margin. However, along this sector, we interpret a probable remnant of underthrusted serpentinized mantle (section 4.2; Figures 10 and 11), similar to that interpreted by Tugend et al. (2014). This fact leads us to map a minimum (overthickened) extent of the necking domain along this sector (Figure 12), although it is not possible to delineate a net coupling line marking the transition from the necking to the HME domain (dashed purple line on Figure 12).

4.3.1.3. Hyperextension and Mantle Exhumation Domain

This domain is related to a positive mid-wavelength Bouguer anomaly (Figure 6c), partly due to the high density serpentinized mantle basement but also due to the rising of the unaltered mantle below it (Figure 7). West of the SR, this domain narrows northward, and north of the 43°N latitude, it is only plainly noticeable by the relict serpentinized mantle ridge, up to 43°20′N (Boillot, Comas et al., 1988). From this latitude on the west margin to north of Galicia, the partial tectonic inversion overprints the former HME domain structure, although a serpentinized mantle unit can be modeled as an underthrusted body in the

compressional front (Figures 10 and 11). The tectonic inversion hampers an accurate identification and delineation of the HME domain (as those accomplished by Sutra et al., 2013 or Tugend et al., 2014) so in the absence of further information to undertake a finer mapping, only a blurry boundary between the necking and the HME domain can be established (Figure 12). North of Galicia, and east of 7°30′W, a positive mid-wavelength Bouguer anomaly is noticeable (*M10*, Figure 6c). This anomaly can be related to the western edge of the mantle exhumation domain mapped by Tugend et al. (2014), Tugend, Manatschal, and Kusznir (2015) on the BAP.

4.3.2. Intense Compressional Deformation Domain

Here are included regions where first-order reverse tectonic features are interpreted and/or modeled, such as the great thrusts identified on the seismic profiles (Figures 8–10) and modeled to fit the gravity curves (Figures 7–11). In addition, this domain encloses also those areas where great magnitude tectonic inversion evidences can be deduced. These last evidences include the following:

1. The greater thickness of the previously, extremely stretched continental crust during the rift episode: In addition to the tectonic inversion evidences in the MPR (Murillas et al., 1990), gravity modeling and previous researches (Álvarez-Marrón et al., 1996; Fernández-Viejo et al., 1998) show that, in the lower continental slope, the continental crust is more than 10 km thick. As margin hyperextension occurred during the Bay of Biscay opening (Tugend et al., 2014), here crustal thickness must have been less than 10 km (Sutra et al., 2013). The fact that the tectonic inversion has thickened the continental crust in the HME domain is then an evidence of intense compressional deformation. From gravity modeling, we can calculate a thickening of the continental crust of at least 2 km north of the SR (in the same order of magnitude as calculated by Boillot et al., 1979) and of ~5 km northwest of Galicia (MPR).
2. The overprinted structure of the HME domain: This domain is clearly identified in the west Galicia and north Iberia margins (e.g., Péron-Pinvidic et al., 2013; Tugend et al., 2014), as well as in the conjugate margin (Thinon et al., 2003). But, along the northwest Galicia margin, this domain appears shortened and thickened (from the north of the SR to the north of Galicia), and there is an apparent absence of a mantle exhumation region. In this work, we have modeled a (postulated) serpentinized mantle unit north of the SR and northwest of the MPR, appearing as a relict wedge underthrusted at the base of the continental crust (Tugend et al., 2014), although its geophysical characteristics and the scarcity of information make difficult to identify it (Fernández-Viejo et al., 2011).

Beyond the ICD domain boundaries, some compressional tectonic features, indicative of a less intense deformation, can be identified. Among others, stand out small subvertical faults related to slight reactivation of continental crust blocks, and soft folding and long wavelength positive bulges, are identified in the SR (Vázquez et al., 2008).

5. Discussion

5.1. Continent-Ocean Boundary Delineation

The location of the continent-ocean boundary (COB) in magma-poor rifted margin is a matter of controversy. Usually, the main criteria for the determination of this limit are as follows:

1. The localization of a distal serpentinized mantle ridge (e.g., Boillot, Winterer et al., 1988): The use of the distal serpentinized mantle ridge to delimit the COB may be ambiguous, as some times there are two parallel ridges, as in the IAP south of the SR (Whitmarsh et al., 1996), and its along-strike continuation is difficult to map in the absence of seismic and sampling criteria. Moreover, the use of the correlation of unconformity between the syn- and postrift sedimentary sequences with the beginning of the continental drift is under discussion (Péron-Pinvidic et al., 2007; Sibuet et al., 2007; Tucholke et al., 2007).
2. The presence of isochrones, related to oceanic accretion (Müller et al., 2008; Sibuet, Monti et al., 2004): The recognition of the first isochrones of the new accreted oceanic crust is ambiguous in magma-poor rifted margins, as some magnetic anomalies can be identified on the exhumed lithospheric mantle (Bronner et al., 2011; Direen et al., 2007; Kornprobst & Chazot, 2016; Nirrengarten et al., 2016; Sayers et al., 2001; Sibuet et al., 2007; Stanton et al., 2016). Moreover, on the west Iberia margin, the beginning of the continental drift occurs during the Cretaceous magnetic quiet lapse.
3. The absence of continental crust (Boillot & Froitzheim, 2001): This proposal of the distal edge of the continental crust as the boundary between the oceanic and the continental domains is approachable for

discrete seismic profiles, but it would result in a complex limit for a regional mapping, as many isolated continental crust blocks are left on the hyperextended region, and much seismic coverage would be needed.

Here we consider the COB as a simplified line that marks the landward edge of the oceanic crust (e.g., Autin et al., 2010; Ball et al., 2013; Sutra et al., 2013), even if the oceanic crust is anomalously thin, like west of Galicia (Davy et al., 2016; Sibuet et al., 1995), probably being part of a complex proto-oceanic domain (Davy et al., 2016; Gillard et al., 2015, 2016). The available information for the present study does not allow differentiating this probable proto-oceanic domain from the steady state oceanic crust. The detailed gravity analysis and modeling addressed here, together with other geophysical, geological, and sampling information, has allowed delineating a continuous and consistent COB (as defined here) along the whole Galicia margin. The only observation of the Bouguer anomaly map is not sufficient to map this border, as values vary from 90 to 350 mGal due to the complex geometry of the margin and of the transition to the oceanic domain (Figure 5a). It was necessary to perform a detailed geophysical data processing and analysis to delineate this limit. Thus, frequency filtering and 2 + 3/4-D modeling from the Bouguer anomaly grid highlighted the effects of the compressional tectonics over the igneous oceanic basement, which is found uplifted and overthrusting at the foot of the slope of the MPR and north and northwest of the SR (Figures 6 and 9–11).

5.2. Role of the Compositional and Structural Inheritance in the Rift Segmentation

The studied area was tentatively divided into different along-strike segments which are from south to north: south IAP segment (SIAP), west Galicia segment (WG), northwest Galicia segment (NWG), and north Iberia segment (NI). Starting from the south, the SIAP segment of the Iberia margin shows relatively narrow stretched and necking domains and a wide HME domain (Figure 12). The transition to the WG segment is made by means of a NW-SE structure (1 at Figure 12), characterized by the Bouguer anomaly gradient *G4* (Figure 5) that connects the SR relative minimums with the *M5* relative maximum over the south IAP (Figures 6b and 6c). On the WG segment, the main features are NNW-SSE directed (Figure 1a, *M1*, *M2*, and gradient bands *G1*–*G2* on Figures 5 and 6), cross-cut by NW-SE and NE-SW features (*G7* and *G8*, Figures 5 and 6) that probably acted as transfer zones during rifting (e.g., Murillas et al., 1990). Northward, there is a complex transition to the north Iberia margin, with an interference of both the main structural directions related to the west and the north Iberia rifts. Thus, the NWG segment is marked by various directional changes on the main margin structures (from NE-SW northwest of the SR to E-W north of the SR, to NE-SW northwest of Galicia; see Figures 5 and 6), also noticeable on detailed quantitative analysis of bathymetric lineaments (Maestro et al., 2017). These orientation changes seem to be favored by NNE-SSW features (2–5 at Figure 12), identified as Bouguer anomaly gradients and morphotectonic lineaments (*G9* and *G10* at Figure 6d; see Figure S1). These NNE-SSW structures may have acted as transfer zones in this margin segment, influenced by the north Iberia margin tectonics, where rift occurs oblique to the main divergence directions in a transtensional stress regime context (e.g., Jammes et al., 2009, and references therein), as is the case of the Gulf of Aden (Bellahsen et al., 2013, and references therein). The structural sketch of this sector of the margin is also similar to those obtained by analog modeling for an oblique rift (Bellahsen et al., 2013, and references therein), probably favored by the preexisting NE-SW Late Triassic-Early Jurassic structures (e.g., Vegas et al., 2016). The NI segment is found east of the last NNE-SSW transfer zone (5, Figure 12). At this sector, the main margin features are approximately E-W directed (Maestro et al., 2017), continuing eastward on the Bay of Biscay (e.g., Roca et al., 2011; Tugend et al., 2014, and references therein).

It seems clear that rift segmentation along the Galicia margin is highly influenced by preexistent rheological discontinuities and tectonic fabric. Many studies have related the influence of first-order rheological heterogeneities on the strain localization during continental rifting and breakup (e.g., Ball et al., 2013; Dunbar & Sawyer, 1989; Manatschal et al., 2015; Muentener & Manatschal, 2006; Sutra & Manatschal, 2012). In the west Galicia margin, both compositional and structural inheritances appear to condition rift development (Chenin et al., 2015; Manatschal et al., 2015). Regarding compositional inheritance, seismic velocity modeling demonstrates that the GIB, where initial Berriasian-Valanginian rift axis was centered (Murillas et al., 1990), originated at the border between two different Paleozoic terrains of the Hercynian belt (Pérez-Gussinyé et al., 2003), which are the Central Iberian and the Ossa-Morena zones (Figure 1b; Capdevila & Mougenot, 1988; Mamet et al., 1991; Manatschal et al., 2015; Martínez Catalán et al., 2009). Moreover, the separation between the WG sector and the SIAP sector is made by means of the NW-SE transfer zone mentioned above (1 on

Figure 12). This transfer zone, evidenced by bathymetry (as it coincides with the southern border of the SR), and gravity anomaly analysis, is approximately located on the Hercynian deformation front (Figure 1b), separating two terrains (Avalonia and Gondwana) with distinct rheological behavior (Manatschal et al., 2015; Martínez Catalán et al., 2009; Mohn et al., 2015). With respect to the structural inheritance, the whole Iberia rift system seems to surround the Hercynian core (Bowling & Harry, 2001; Capdevila & Mougenot, 1988; Chenin et al., 2015; Lefort & Haworth, 1979). Rifting is apparently favored by first-order "weak" structures corresponding to Hercynian thrust fronts and strike-slip faults (Figure 1b) but also possibly conditioned by prerift (Triassic and Late Triassic-Early Jurassic) strike-slip faulting (Sopeña et al., 1988; Vegas et al., 2016; Ziegler, 1982). This preexistent fabric seems to control the main structural directions under extension (evidenced by the different gravity anomaly lineaments described above), at both the northern and western segments, as these coincide approximately with the main thrusts and strike-slip fault directions observed onshore (Figures 1a and 1b; Ramírez et al., 2006). The influence of the Triassic tectonic event (e.g., Sopeña et al., 1988) on the margin segmentation is evident in the NNE-SSW trending structures (*G9* and *G10* in Figure 6d and 2–5 in Figure 12). These structures probably acted as transform faults during the oblique rifting north of the SR and northwest of Galicia, allowing the changes on the main structural directions as rifting progressed toward the north Iberia margin. The NNE-SSW structural direction manifests also on land (e.g., Rockwell et al., 2009), as left-lateral strike-slip faults under the compressional regime (De Vicente, 2004; De Vicente et al., 2008; De Vicente & Vegas, 2009). The NE-SW and NW-SE Late Triassic-Early Jurassic rift structures (Vegas et al., 2016) act as strike-slip fractures in the west Iberia margin; meanwhile, NE-SW structures behave as normal faults in the NWG segment during the Cretaceous rifting.

5.3. Influence of Rift Architecture on the Partial Tectonic Inversion of the Margin

Rift-related architecture has been proven to influence the margin tectonic inversion and in subsequent subduction and collision processes. In this context, the HME domain plays a key role, as the serpentinized mantle unit acts as a detachment surface, facilitating the inversion processes (e.g., Chenin et al., 2017; Tugend et al., 2014, and references therein).

Our observations of the deep structure of the Galicia continental margin allow us to propose a simplified conceptual model for the initiation of the tectonic inversion of the magma-poor rifted margin north and northwest of Galicia (Figure 13). In this model, the initial HME domain is the first region to be inverted and which accommodates most of the compressional deformation, as mantle partial serpentinization leads to weakening, making this domain prone to compressive deformation (Lundin & Doré, 2011). The location of the compressional deformation in this region is favored by the reactivation of the former detachment at the base of the continental crust, which originated during the rifting episode (Figure 13a). At the outer flank of the HME domain, the serpentinized peridotite ridge acts as a weakness zone that favors the nucleation of a thrust under the compressional regime (Figure 13b; Lundin & Doré, 2011; Tugend et al., 2014), such as that observed west and north of the SR (Figures 7–9). Some deformation can develop also toward the continent in the serpentinized mantle unit, as those convex morphologies modeled at the GM2–GM4 that could be related to thrusts (Figures 7–9). With the compressional deformation progress, the tectonic inversion propagates along the detachment surface toward the continent in the HME domain, and some normal faults are also reactivated in the continental basement. The proximal oceanic crust is anomalously thin and may be also underlined by serpentinized peridotite, entailing a weakness zone under the compressional regime (Figures 7–9; Davy et al., 2016; Sibuet et al., 1995; Thinon et al., 2003; Whitmarsh et al., 1996). As compression advances, new thrust features can develop in this thin and weak oceanic crust, with a foreland shifting of the deformation front (Figure 13c). This result on the formation of oceanic basement in sequence thrusts as those observed north of the SR and north and northwest of Galicia (Figures 9–11). If tectonic inversion progresses, the reactivation of previous normal faults on the continental basement would advance toward the necking and stretching domains, leading to a deformation of the postrift sedimentary cover, as previously noticed northwest of Galicia (Murillas et al., 1990) and in the SR (Vázquez et al., 2008).

The compressional belt bordering the SR and the northwestern margin of Galicia can be considered as an intermediate stage between a hyperextended margin and a "continental margin type" ophiolitic belt (Dilek & Furnes, 2011). If compression had progressed to a collisional orogeny here, the remnants of the serpentinized mantle ridge, together with the overthrusted oceanic basement blocks, could have been obducted in the accretionary prism and exposed afterward as an ophiolitic belt such as those observed at the Pyrenees

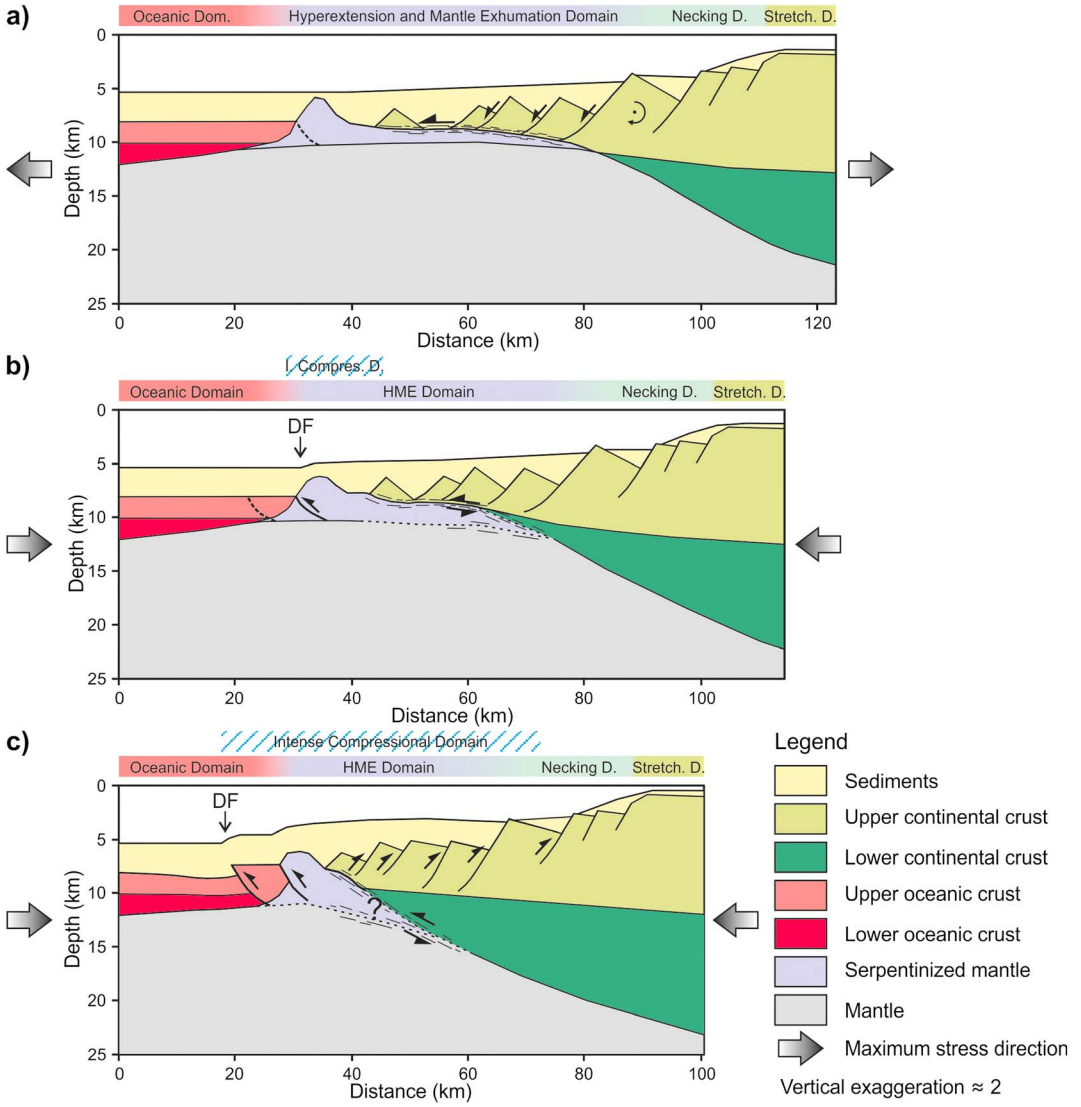

Figure 13. Simplified conceptual model for the initiation of the tectonic inversion of the north and northwest Galicia margin. (a) Starting point, at the end of the rifting episode. (b) Initiation of the tectonic inversion. Most of the compressional deformation is mainly assumed by the serpentinized mantle unit and by the lithospheric detachment, which is reversely reactivated. A thrust is originated on the distal flank of the peridotite ridge. (c) Present stage of the tectonic inversion of the margin. When most of the serpentinized unit has been consumed by the tectonic inversion of the detachment, compressional deformation propagates toward the foreland by the generation of new thrusts affecting the proximal thin and weak oceanic crust. Tectonic compressional deformation progresses also toward the continent by the partial inversion of previous normal faults. DF, deformation front.

(e.g., Jammes et al., 2009; Lagabrielle et al., 2010; Mouthereau et al., 2014) and the Alps (Beltrando et al., 2014; Manatschal, 2004; Mohn et al., 2014; Whitmarsh et al., 1993). Conversely, the underthusted remnants of the serpentinized mantle body would become a component of the subducted part of the orogeny (Chenin et al., 2017).

6. Conclusions

The use of gravity analysis, in combination with seismic and sampling data, is an adequate methodology for performing structural domain mapping. On the northwestern Galicia margin, where no good coverage of seismic information is available, detailed gravity analysis has allowed an extrapolation of the seismic and sampling constrained interpretations, and a first approach to this mapping is achieved. This methodology is also useful for determining the across and along-strike structure of the margin.

The transition from continental to oceanic domain west of Galicia and south of 42°20′N latitude is very progressive. The necking and the HME domains were mapped on this sector of the margin. The HME domain narrows northward with a wedge shape from approximately 50 km wide at 42°N latitude until it disappears north of 43°N. The serpentinized mantle ridge prolongs until 43°20′N, with no surficial evidence of its existence further north of the SR, where a rotation of the main tectonic features is observed. From south to north, the serpentinized mantle ridge displays morphological variations, from being symmetrical in the south to show a steeper distal flank northward, where its contact with the oceanic crust occurs through overthrusting. North of the SR and the GIB, and at the foot of the MPR, the continent-ocean transition is more abrupt and is modeled as a major continental basement thrust over the oceanic one, with an underthrusted serpentinized mantle unit at the base of the continental crust. Here the boundary between the necking and the HME domain is hardly established, as it is overprinted by the tectonic inversion of the margin.

The detailed gravity analysis has allowed a continuous mapping of the crustal and structural domains along the margin and strengthens the utility of the gravity method for such mapping. As a result, an accurate delineation of the COB has been mapped, as well as the coupling line that marks the limit between the necking and the HME domains. Because a superimposed ICD domain also has been mapped, a compressional deformation front has been delineated.

The studied area has been divided in four different segments, according to their compositional and structural characteristics: SIAP, WG, NWG, and NI. Different sectors seem to develop in distinct Hercynian belt zones, with the segmentation favored by preexisting weak zones that act as first-order transfer zones during rifting. In turn, rift architecture strongly conditions its evolution under the subsequent compressional regime, with the HME domain focusing most of the compressive deformation. The observations made on the deep structure of the Galicia continental margin have led us to propose a simplified model for the initiation of the tectonic inversion of a hyperextended rift margin. In accordance with previous works, the HME domain accommodates most of the compressional deformation. As tectonic inversion progresses, the first oceanic basement, anomalously thin and underlined by serpentinized mantle, is faulted and overthrusts, remaining uplifted at the base of the continen\tal slope.

Acknowledgments
The original data sets used in this work were obtained during the Spanish EEZ Project and ERGAP Project. Official EEZ charts are published by Martín-Dávila et al. (2012). ERGAP Project data are accessible via http://gma.icm.csic.es/sites/default/files/geowebs/OLsurveys/index.htm#. We want to thank the various captains, officers, and crewmembers of the R/V *Hespérides* who operated the EEZ cruises carried out from 2001 to 2009. We also thank "Unidad de Tecnología Marina" (CSIC) for their indispensable support during the cruises. The GMT5 software system from Wessel et al. (2013) was invaluable for conducting the spectral analysis and filtering. We want to express many thanks to L. Lavier, P. Ball and an anonymous reviewer for their constructive revisions and suggestions that certainly improved the final manuscript.

References

Álvarez-Marrón, J., Pérez-Estaún, A., Dañobeitia, J. J., Pulgar, J., Martínez Catalán, J., Marcos, A., et al. (1996). Seismic structure of the northern continental margin of Spain from ESCIN deep seismic profiles. *Tectonophysics*, *264*(1–4), 153–174. https://doi.org/10.1016/S0040-1951(96)00124-2

Álvarez-Marrón, J., Rubio, E., & Torne, M. (1997). Subduction-related structures in the north Iberian margin. *Journal of Geophysical Research*, *102*, 22,497–22,511. https://doi.org/10.1029/97JB01425

Alves, T. M., Moita, C., Cunha, T., Ullnaess, M., Myklebust, R., Monteiro, J. H., & Manuppella, G. (2009). Diachronous evolution of Late Jurassic-Cretaceous continental rifting in Northeast Atlantic (west Iberian margin). *Tectonics*, *28*, TC4003. https://doi.org/10.1029/2008TC002337

Autin, J., Leroy, S., Beslier, M.-O., d'Acremont, E., Razin, P., Ribodetti, A., et al. (2010). Continental breakup history of a deep magma-poor margin based on seismic reflection data (northeastern Gulf of Aden margin, offshore Oman). *Geophysical Journal International*, *180*(2), 501–519. https://doi.org/10.1111/j.1365-246X.2009.04424.x

Ball, P., Eagles, G., Ebinger, C., McClay, K., & Totterdell, J. (2013). The spatial and temporal evolution of strain during the separation of Australia and Antarctica. *Ceochemistry, Geophysics and Geosystems*, *14*, 2771–2799. https://doi.org/10.1002/ggge.20160

Barton, P. J. (1986). The relationship between seismic velocity and density in the continental crust—A useful constraint? *Geophysical Journal of the Royal Astronomical Society*, *87*(1), 195–208. https://doi.org/10.1111/j.1365-246X.1986.tb04553.x

Bellahsen, N., Husson, L., Autin, J., Leroy, S., & d'Acremont, E. (2013). The effect of thermal weakening and buoyancy forces on rift localization: Field evidences from the Gulf of Aden oblique rifting. *Tectonophysics*, *607*, 80–97. https://doi.org/10.1016/j.tecto.2013.05.042

Beltrando, M., Manatschal, G., Mohn, G., Dal Piaz, G. V., Brovarone, A. V., & Massini, E. (2014). Recognizing remnants of magma-poor rifted margins in high-pressure orogenic belts: The Alpine case study. *Earth-Science Reviews*, *131*, 88–115. https://doi.org/10.1016/j.earscirev.2014.01.001

Boillot, G., Auxietre, J. L., Dunand, J. P., Dupeuble, P. A., & Mauffret, A. (1979). The northwestern Iberian Margin: A Cretaceous passive margin deformed during Eocene. In M. Talwani, W. W. Hay, & W. B. F. Ryan (Eds.), *Deep Drilling Results in the Atlantic Ocean: Continental Margins and Paleoenvironment. Maurice Ewing Maurice Ewing Series* (pp. 138–153). Washington, DC: American Geophysical Union.

Boillot, G., Beslier, M. O., Krawczyk, C. M., Rappin, D., & Reston, T. J. (1995). The formation of passive margins: Constraints from the crustal structure and segmentation of the deep Galicia margin, Spain. In R. A. Scrutton et al. (Eds.), *The tectonics, sedimentation and paleoceanography of the North Atlantic Region*, *Special Publications* (pp. 71–91). London: Geological Society.

Boillot, G., Comas, M. C., Girardeau, J., Kornprobst, J., Loreau, J. P., Malod, J., et al. (1988). Preliminary results of the GALINAUTE cruise dives of the submersible 'Nautile' on the West Galicia margin, Spain. In G. Boillot, E. L. Winterer, & A. W. Meyer (Eds.), *Proceedings of the Ocean Drilling Program, Scientific Results 103* (pp. 37–51). College Station, TX: Ocean Drilling Program. https://doi.org/10.2973/odp.proc.sr.103.118.1988

Boillot, G., & Froitzheim, N. (2001). Non-volcanic rifted margins, continental breakup and the onset of sea-floor spreading: Some outstanding questions. In R. C. L. Wilson, et al. (Eds.), *Non-volcanic rifting of continental margins: A comparison of evidence from land and sea*, *Special Publications* (Vol. 187, pp. 9–30). London: Geological Society. https://doi.org/10.1144/GSL.SP.2001.187.01.02

Boillot, G., & Malod, J. (1988). The north and north-west Spanish continental margin: A review. *Revista de la Sociedad Geológica de España*, *1*, 295–316.

Boillot, G., Recq, M., Winterer, E. L., Applegate, J., Baltuck, M., Bergen, J. A., et al. (1987). Tectonic denudation of the upper mantle along passive margin: A model based on drilling results (Ocean Drilling Program leg 103, western Galicia margin, Spain). *Tectonophysics*, *132*(4), 335–342. https://doi.org/10.1016/0040-1951(87)90352-0

Boillot, G., Winterer, E. L., & Meyer, A. W. (1988). *Proceedings of the Ocean Drilling Program, scientific results* (Vol. 103). College Station, TX: Ocean Drilling Program.

Bowling, J. C., & Harry, D. L. (2001). Geodynamic models of continental extension and the formation of non-volcanic rifted continental margins. In R. C. L. Wilson, et al. (Eds.), *Non-volcanic rifting of continental margins: A comparison of evidence from land and sea*, *Special Publications* (Vol. 187, pp. 511–536). London: Geological Society.

Brocher, T. M. (2005). Empirical relations between elastic wavespeeds and density in the Earth's crust. *Bulletin of the Seismological Society of America*, *95*(6), 2081–2092. https://doi.org/10.1785/0120050077

Bronner, A., Sauter, D., Mantschal, G., Péron-Pinvidic, G., & Munschy, M. (2011). Magmatic breakup as an explanation for magnetic anomalies at magma-poor rifted margins. *Nature Geoscience*, *4*(8), 549–553. https://doi.org/10.1038/NGEO1201

Brune, S., Heine, C., Pérez-Gussinyé, M., & Sobolev, S. V. (2014). Rift migration explains continental margin asymmetry and crustal hyper-extension. *Nature Communications*, *5*, 4014. https://doi.org/10.1038/ncomms5014

Capdevila, R., & Mougenot, D. (1988). Pre-Mesozoic basement of the western Iberian continental margin and its place in the Variscan Belt. In G. Boillot, E. L. Winterer, & A. W. Meyer (Eds.), *Proceedings of the Ocean Drilling Program, scientific results 103* (pp. 3–12). College Station, TX: Ocean Drilling Program. https://doi.org/10.2973/odp.proc.sr.103.116.1988

Capote, R., Muñoz, J. A., Simón, J. L., Liesa, C. L., & Arlegui, L. E. (2002). Alpine tectonics I: The alpine system north of the Betic cordillera. In W. Gibbons & T. Moreno (Eds.), *The geology of Spain* (pp. 367–400). London: Geological Society.

Carbó, A., Muñoz, A., Llanes, P., Álvarez, J., & ZEE Working Group (2003). Gravity analysis offshore the Canary Islands from a systematic survey. *Marine Geophysical Researches*, *24*, 113–127.

Chenin, P., Manatschal, G., Lavier, L. L., & Errat, D. (2015). Assessing the impact of orogenic inheritance on the architecture, timing and magmatic budget of the North Atlantic rift system: A mapping approach. *Journal of the Geological Society*, *172*(6), 711–720. https://doi.org/10.1144/jgs2014-139

Chenin, P., Manatschal, G., Picazo, S., Müntener, O., Karner, G., Johnson, C., & Ulrich, M. (2017). Influence of the architecture of magma-poor hyperextended rifted margins on orogens produced by the closure of narrow versus wide oceans. *Geosphere*, *13*(2), 559–576. https://doi.org/10.1130/GES01363.1

Christensen, N. I., & Mooney, W. D. (1995). Seismic velocity structure and composition of the continental crust: A global view. *Journal of Geophysical Research*, *100*, 9761–9788. https://doi.org/10.1029/95JB00259

Clark, S. A., Sawyer, D. S., Austin, J. A. Jr., Christeson, G. L., & Nakamura, Y. (2007). Characterizing the Galicia Bank-southern Iberia abyssal plain rifted margin segment boundary using multichannel seismic and ocean bottom seismometer data. *Journal of Geophysical Research*, *112*, B03408. https://doi.org/10.1029/2006JB004581

Córdoba, D., Banda, E., & Ansorge, J. (1987). The Hercynian crust in northwestern Spain: A seismic survey. *Tectonophysics*, *132*(4), 321–333. https://doi.org/10.1016/0040-1951(87)90351-9

Davy, R. G., Minshull, T. A., Bayrakci, G., Bull, J. M., Klaeschen, D., Papenberg, C., et al. (2016). Continental hyperextension, mantle exhumation and thin oceanic crust at the continent-ocean transition, West Iberia: New insights from wide-angle seismic. *Journal of Geophysical Research: Solid Earth*, *121*, 3177–3199. https://doi.org/10.1002/2016JB012825

De Vicente, G. (2004). Estructura Alpina del Antepaís Ibérico. In J. A. Vera (Ed.), *Geología de España* (pp. 587–634). Madrid. Sociedad Geológica de España and Instituto Geológico y Minero de España.

De Vicente, G., Cloetingh, S., Muñoz-Martín, A., Olaiz, A., Stich, D., Vegas, R., et al. (2008). Inversion of moment tensor focal mechanisms for active stresses around the microcontinent Iberia: Tectonic implications. *Tectonics*, *27*, TC1009. https://doi.org/10.1029/2006TC002093

De Vicente, G., & Vegas, R. (2009). Large-scale distributed deformation controlled topography along the western Africa-Eurasia limit: Tectonic constraints. *Tectonophysics*, *474*(1-2), 124–143. https://doi.org/10.1016/j.tecto.2008.11.026

Dean, S. M., Minshull, T. A., Whitmarsh, R. B., & Louden, K. E. (2000). Deep structure of the ocean-continent transition in the southern Iberia abyssal plain from seismic refraction profiles: The IAM-9 transect at 40°20′N. *Journal of Geophysical Research*, *105*, 5859–5885. https://doi.org/10.1029/1999JB900301

Díaz, J., & Gallart, J. (2009). Crustal structure beneath the Iberian Peninsula and surrounding waters: A new compilation of deep seismic sounding results. *Physics of the Earth and Planetary Interiors*, *173*(1-2), 181–190. https://doi.org/10.1016/j.pepi.2008.11.008

Dilek, Y., & Furnes, H. (2011). Ophiolite genesis and global tectonics: Geochemical and tectonic fingerprint of ancient oceanic lithosphere. *Geological Society of America Bulletin*, *123*(3-4), 387–411. https://doi.org/10.1130/B30446.1

Direen, N. G., Borissova, I., Stagg, H. M. J., Colwell, J. B., & Symonds, P. A. (2007). Nature of the continent-ocean transition zone along the southern Australian continental margin: A comparison of the Naturaliste Plateau, SW Australia, and the central Great Australian Bight sectors. In G. Karner, G. Manatschal, & L. Pinheiro (Eds.), *Imaging, mapping and modelling continental lithosphere extension and breakup*, *Special Publications* (Vol. 282, 282, pp. 239–263). London: Geological Society. https://doi.org/10.1144/SP282.12

Doré, T., & Lundin, E. (2015). Hyperextended continental margins—Knowns and unknowns. *Geology*, *43*(1), 95–96. https://doi.org/10.1130/focus012015.1

Dunbar, J. A., & Sawyer, D. S. (1989). How preexisting weaknesses control the style of continental breakup. *Journal of Geophysical Research*, *94*, 7278–7492. https://doi.org/10.1029/JB094iB06p07278

Ercilla, G., García-Gil, S., Estrada, F., Gràcia, E., Vizcaino, A., T, J., et al. (2008). High resolution seismic stratigraphy of the Galicia Bank Region and neighbouring abyssal plains (NW Iberian continental margin). *Marine Geology*, *249*(1-2), 108–127. https://doi.org/10.1016/j.margeo.2007.09.009

Fernández-Viejo, G., Gallart, J., Pulgar, J. A., Gallastegui, J., Dañobeitia, J. J., & Córdoba, D. (1998). Crustal transition between continental and oceanic domains along the north Iberian margin from wide angle seismic and gravity data. *Geophysical Research Letters*, *25*, 4249–4252. https://doi.org/10.1029/1998GL900149

Fernández-Viejo, G., Gallastegui, J., Pulgar, J. A., & Gallart, J. (2011). The MARCONI reflection seismic data: A view into the eastern part of the Bay of Biscay. *Tectonophysics*, *508*(1-4), 34–41. https://doi.org/10.1016/j.tecto.2010.06.020

Gillard, M., Autin, J., Manatschal, G., Sauter, D., Munschy, M., & Schaming, M. (2015). Tectonomagmatic evolution of the final stages of rifting along the deep conjugate Australian-Antarctic magma-poor rifted margins: Constraints from seismic observations. *Tectonics*, *34*, 753–783. https://doi.org/10.1002/2015TC003850

Gillard, M., Manatschal, G., & Autin, J. (2016). How can asymmetric detachment faults generate symmetric ocean continent transitions? *Terra Nova*, *28*(1), 27–34. https://doi.org/10.1111/ter.12183

González, A., Córdoba, D., & Vales, D. (1999). Seismic crustal structure of Galicia continental margin, NW Iberian Peninsula. *Geophysical Research Letters*, *26*, 1061–1064. https://doi.org/10.1029/1999GL900193

Grimaud, S., Boillot, G., Collete, B., Mauffret, A., Miles, P. R., & Roberts, D. B. (1982). Western extension of the Iberian-European plate boundary during the early Cenozoic (Pyrenean) convergence: A new model. *Marine Geology*, *45*(1-2), 63–77. https://doi.org/10.1016/0025-3227(82)90180-3

Groupe Galice (1979). The continental margin of Galicia and Portugal, acoustic stratigraphy, dredge stratigraphy and structural evolution. In B. F. Ryan & J. C. Sibuet (Eds.), *Proceedings of the Deep Sea Drilling Project*, (Vol. 47, pp. 633–662). Washington, DC.

Jammes, S., Manatschal, G., Lavier, L., & Masini, E. (2009). Tectonosedimentary evolution related to extreme crustal thinning ahead of a propagating ocean: Example of the western Pyrenees. *Tectonics*, *28*, TC4012. https://doi.org/10.1029/2008TC002406

Jané, G., Llave, E., Maestro, A., López-Martínez, J., Ercilla, G., Barnolas, A., et al. (2011). Morphologic characterization of the Biscay abyssal plain deep-sea channels system. *Geogaceta*, *50-2*, 141–144.

Kane, M. F. (1962). A comprehensive system of terrain corrections using a digital computer. *Geophysics*, *27*(4), 455–462. https://doi.org/10.1190/1.1439044

Karner, G., & Watts, A. (1983). Gravity anomalies and flexure of the lithosphere at mountain ranges. *Journal of Geophysical Research*, *88*, 10,449–10,477. https://doi.org/10.1029/JB088iB12p10449

Kornprobst, J., & Chazot, G. (2016). Peridotites and mafic igneous rocks at the foot of the Galicia margin: An oceanic or continental lithosphere? A discussion. *Boletín Geológico y Minero*, *127*(2/3), 317–332.

Krawczyk, C. M., Reston, T. J., Beslier, M. O., & Boillot, G. (1996). Evidence for detachment tectonics on the Iberia abyssal plain rifted margin. In R. B. Whitmarsh, et al. (Eds.), *Proceedings of the Ocean Drilling Program, scientific results* (Vol. 149, pp. 603–615). College Station, TX: Ocean Drilling Program. https://doi.org/10.2973/odp.proc.sr.149.244.1996

Lagabrielle, Y., Labaume, P., & de Saint-Banquat, M. (2010). Mantle exhumation, crustal denudation and gravity tectonics during cretaceous rifting in the Pyrenean realm (SW Europe): Insights from the geological setting of the lherzolite bodies. *Tectonics*, *29*, TC4012. https://doi.org/10.1029/2009TC002588

Lavier, L. L., & Manatschal, G. (2006). A mechanism to thin the continental lithosphere at magma-poor margins. *Nature*, *440*(7082), 324–328. https://doi.org/10.1038/nature04608

Lefort, J. P., & Haworth, R. T. (1979). The age and origin of the deepest correlative structures recognized o_ Canada and Europe. *Tectonophysics*, *59*(1-4), 139–150. https://doi.org/10.1016/0040-1951(79)90042-8

Louden, K. E., & Chian, D. (1999). The deep structure of non-volcanic rifted continental margins. *Philosophical Transactions of the Royal Society of London A*, *357*, 767–805.

Ludwig, W. J., Nafe, J. E., & Drake, C. L. (1970). Seismic refraction. In A. E. Maxwell (Ed.), *The sea* (Vol. 4, pp. 53–84). New York: Wiley-Interscience.

Lundin, E. R., & Doré, A. G. (2011). Hyperextension, serpentinization and weakening: A new paradigm for rifted margin compressional deformation. *Geology*, *39*(4), 347–350. https://doi.org/10.1130/G31499.1

Maestro, A., Jané, G., Llave, E., López-Martínez, J., Bohoyo, F., & Druet, M. (2017). The role of tectonic inheritance in the morphostructural evolution of the Galicia continental margin and adjacent abyssal plains from digital bathymetric model (DBM) analysis (NW Spain). *International Journal of Earth Sciences*. https://doi.org/10.1007/s00531-017-1531-4

Malod, J. A., & Mauffret, A. (1990). Iberian plate motions during the Mesozoic. *Tectonophysics*, *184*(3-4), 261–278. https://doi.org/10.1016/0040-1951(90)90443-C

Malod, J. A., Murillas, J., Kornprobst, J., & Boillot, G. (1993). Oceanic lithosphere at the edge of a Cenozoic active continental margin (northwest slope of the Galicia Bank, Spain). *Tectonophysics*, *221*(2), 195–206. https://doi.org/10.1016/0040-1951(93)90332-E

Mamet, B., Comas, M. C., & Boillot, G. (1991). Late Paleozoic basin on the West Galicia Atlantic margin. *Geology*, *19*, 738–741.

Manatschal, G. (2004). New models for evolution of magma poor rifted margins based on a review of data and concepts from the West Iberia and the Alps. *International Journal of Earth Sciences*, *93*(3), 432–466. https://doi.org/10.1007/00531-004-0394-7

Manatschal, G., & Bernoulli, D. (1999). Architecture and tectonic evolution of non-volcanic margins: Present day Galicia and ancient Adria. *Tectonics*, *18*, 1099–1119. https://doi.org/10.1029/1999TC900041

Manatschal, G., Lavier, L., & Chenin, P. (2015). The role of inheritance in structuring hyperextended rift systems: Some considerations based on observations and numerical modelling. *Gondwana Research*, *27*(1), 140–164. https://doi.org/10.1016/j.gr.2014.08.006

Martín-Dálvila, J., Catalán, M., Larrán, M., Sección de Hidrografía del IHM, Carbó, A., Mulñoz-Martín, A., et al. (2012). Zona económica exclusiva española (ZEEE). Margen continental gallego: Mapas generales de batimetría, de anomalías geomagnéticas, gravimétricas de Aire Libre y Bouguer, geomorfológico y mosaico de imágenes de reflectividad. Ministerio de Defensa de España. Secretaría General Técnica (44 p.).

Martínez Catalán, J. R., Arenas, R., Abati, J., Sánchez Martínez, S., Díaz García, F., Fernández Suárez, J., et al. (2009). A rootless suture and the loss of the roots of a mountain chain: The Variscan belt of NW Iberia. *Comptes Rendus Geoscience*, *341*(2-3), 114–126. https://doi.org/10.1016/j.crte.2008.11.004

Medialdea, T., Somoza, L., Bohoyo, F., Vázquez, J. T., Vegas, R., Patriat, M., et al. (2009). Compresión cenozoica en la Cuenca de la Unión y Monte Submarino Armoricano (Llanura Abisal de Vizcaya). 6th Symposium on the Atlantic Iberian Margin, Abstract book (pp. 77–80). https://doi.org/10.13140/2.1.4439.0089

Mohn, G., Karner, G. D., Manatschal, G., & Johnson, C. A. (2015). Structural and stratigraphic evolution of the Iberia-Newfoundland hyperextended rifted margin: A quantitative modelling approach. In G. M. Gibson, F. Roure, & G. Manatschal (Eds.), *Sedimentary basins and crustal processes at continental margins: From modern hyperextended margins to deformed ancient analogues*. Geological Society, London, *Special Publications*, 413. https://doi.org/10.1144/SP413.9

Mohn, G. G., Manatschal, M. B., & Haupert, I. (2014). The role of rift-inherited hyper-extension in Alpine-type orogens. *Terra Nova*, *26*(5), 347–353. https://doi.org/10.1111/ter.12104

Montadert, L., Winnock, E., Detiel, J. R., & Grau, G. (1974). Continental margins of Galicia-Portugal and Bay of Biscay. In C. A. Burk & C. L. Drake (Eds.), *The geology of continental margins* (pp. 323–342). New York Springer. https://doi.org/10.1007/978-3-662-01141-6_24

Mouthereau, F., Filleaudeau, P. Y., Vacherat, A., Pik, R., Lacombe, O., Fellin, M. G., et al. (2014). Placing limits to shortening evolution in the Pyrenees: Role of margin architecture and implications for the Iberia/Europe convergence. *Tectonics*, *33*, 2283–2314. https://doi.org/10.1002/2014TC003663

Muentener, O., & Manatschal, G. (2006). High degrees of melt extraction recorded by spinel harzburgite of the Newfoundland margin: The role of inheritance and consequences for the evolution of the southern North Atlantic. *Earth and Planetary Science Letters*, *252*(3–4), 437–452. https://doi.org/10.1016/j.epsl.2006.10.009

Müller, R. D., Sdrolias, M., Gaina, C., & Roest, W. R. (2008). Age, spreading rates and spreading symmetry of the world's ocean crust. *Geochemistry, Geophysics, Geosystems*, *9*, Q04006. https://doi.org/10.1029/2007GC001743

Muñoz-Martín, A., de Vicente, G., Fernández-Lozano, J., Cloethingh, S., Willongshofer, E., Sokoutis, D., & Beekman, F. (2010). Spectral analysis of the gravity and elevation along the western Africa-Eurasia plate tectonic limit: Continental versus oceanic lithospheric signals. *Tectonophysics*, *495* (3–4). https://doi.org/10.1016/j.tecto.2010.09.036

Murillas, J., Mougenot, D. G., Boillot, G., Comas, M. C., Banda, E., & Mauffret, A. (1990). Structure and evolution of the Galicia interior basin (Atlantic western Iberian continental margin). *Tectonophysics*, *184*, 297–319.

Naggy, D. (1966). The gravitational attraction of a right rectangular prism. *Geophysics*, *31*(2).

Naliboff, J. B., Biter, S. H., Péron-Pinvidic, G., Osmundsen, P. T., & Tetreault, J. (2017). Complex fault interaction controls continental rifting. *Nature Communications*, *8*(1), 1179. https://doi.org/10.1038/s41467-017-00904-x

Nirrengarten, M., Manatschal, G., Tugend, J., Kusznir, N. J., & Sauter, D. (2016). Nature and origin of the J-magnetic anomaly offshore Iberia-Newfoundland: Implications for plate reconstructions. *Terra Nova*, *29*(1), 20–28. https://doi.org/10.1111/ter.12240

Olivet, J. L. (1996). La cinématique de la plaque Ibérique. *Bulletin des Centres de Recherches Exploration-Production Elf-Aquitaine*, *20*, 131–195.

Pérez-Estaún, A., & Bea, F. (2004). Macizo Ibérico. In J. A. Vera (Ed.), *Geología de España* (pp. 19–230). Madrid. Sociedad Geológica de España and Instituto Geológico y Minero de España.

Pérez-Gussinyé, M., Ranero, C. R., & Reston, T. J. (2003). Mechanisms of extension at nonvolcanic margins: Evidence from the Galicia interior basin, west of Iberia. *Journal of Geophysical Research*, *108*(B5), 2245. https://doi.org/10.1029/2001JB000901

Pérez-Gussinyé, M., & Reston, T. J. (2001). Rheological evolution during extension at nonvolcanic rifted margins: Onset of serpentinization and development of detachments leading to continental breakup. *Journal of Geophysical Research*, *106*, 3961–3975. https://doi.org/10.1029/2000JB900325

Péron-Pinvidic, G., & Manatschal, G. (2009). The final rifting evolution at deep magma-poor passive margins from Iberia-Newfoundland: A new point of view. *International Journal of Earth Sciences*, *98*(7), 1581–1597. https://doi.org/10.1007/s00531-008-0337-9

Péron-Pinvidic, G., Manatschal, G., Minshull, T. A., & Sawyer, D. S. (2007). Tectonosedimentary evolution of the deep Iberia-Newfoundland margins: Evidence for a complex breakup history. *Tectonics*, *26*, TC2011. https://doi.org/10.1029/2006TC001970

Péron-Pinvidic, G., Manatschal, G., & Osmundsen, P. T. (2013). Structural comparison of archetypal Atlantic rifted margins: A review of observations and concepts. *Marine and Petroleum Geology*, *43*, 21–47. https://doi.org/10.1016/j.marpetgeo.2013.02.002

Pickup, S. L. B., Whitmarsh, R. B., Fowler, C. M. R., & Reston, T. J. (1996). Insight into the nature of the ocean-continent transition west of Iberia from a deep multichannel seismic reflection profile. *Geology*, *24*(12), 1079–1082. https://doi.org/10.1130/0091-7613(1996)024%3C1079:IITNOT%3E2.3.CO;2

Ramírez, M. S., Lucini, J., Plaza, J., Carreño, E., Martínez, J. M., & de Vicente, G. (2006). Proyecto Prior: Determinación de fallas de Primer Orden mediante análisis integrado de datos geológicos. Colección Otros Documentos, Consejo de Seguridad Nacional, n. 15.2006: pp. 312.

Reguzzoni, M., & Sampietro, D. (2015). GEMMA: An Earth crustal model based on GOCE satellite data. *International Journal of Applied Earth Observation and Geoinformation*, *35*, 31–43. https://doi.org/10.1016/j.jag.2014.04.002

Reston, T. J. (2009). The structure, evolution and symmetry of the magma-poor rifted margins of the North and Central Atlantic: A synthesis. *Tectonophysics*, *468*(1-4), 6–27. https://doi.org/10.1016/j.tecto.2008.09.002

Reston, T. J., Krawczyk, C. M., & Klaeschen, D. (1996). The S reflector west of Galicia (Spain): Evidence from pre-stack depth migration for detachment faulting during continental break-up. *Journal of Geophysical Research*, *101*, 8075–8091. https://doi.org/10.1029/95JB03466

Roca, E., Muñoz, J. A., Ferrer, O., & Ellouz, N. (2011). The role of the Bay of Biscay Mesozoic extensional structure in the configuration of the Pyrenean orogen: Constraints from the MARCONI deep seismic reflection survey. *Tectonics*, *30*, TC2001. https://doi.org/10.1029/2010TC002735

Rockwell, T., Fonseca, J., Madden, C., Dawson, T., Owen, L. A., Vilanova, S., & Figueiredo, P. (2009). Palaeoseismology of the Vilariça segment of the Manteigas-Bragança fault in northeastern Portugal. *Geological Society Special Publication*, *316*(1), 237–258. https://doi.org/10.1144/SP316.15

Sampietro, D., Reguzzoni, M., & Negretti, N. (2013). The GEMMA crustal model: First validation and data distribution. ESA SP-722.

Sandwell, D. T., Müller, R. D., Smith, W. H. F., Garcia, E., & Francis, R. (2014). New global marine gravity model from CryoSat-2 and Jason-1 reveals buried tectonic structure. *Science*, *346*(6205), 65–67. https://doi.org/10.1126/science.1258213

Sayers, J., Symonds, P., Direen, N. G., & Bernardel, G. (2001). Nature of the continent-ocean transition on the non-volcanic rifted margin of the central Great Australian Bight. In R. C. L. Wilson, R. B. Whitmarsh, & N. Froitzheim (Eds.), *Non-volcanic rifting of continental margins: A comparison of evidence from land and sea*, *Special Publications* (Vol. 187, pp. 51–76). London: Geological Society.

Sibuet, J. C., & Collete, B. J. (1991). Triple junctions of Bay of Biscay and North Atlantic: New constraints on the kinematic evolution. *Geology*, *19*(5), 522–525. https://doi.org/10.1130/0091-7613(1991)019%3C0522:TJOBOB%3E2.3.CO;2

Sibuet, J. C., Louvel, V., Whitmarsh, R. B., White, R. S., Horsefield, S. J., Sichler, B., et al. (1995). Constraints on rifting processes from refraction and deep-tow magnetic data: The example of the Galicia continental margin (West Iberia). In E. Banda, et al. (Eds.), *Rifted ocean-continent boundaries* (pp. 197–217). Dordrecht, Netherlands: Kluwer Academic Publishers. https://doi.org/10.1007/978-94-011-0043-4_11

Sibuet, J. C., Mazé, J. P., Amortilla, P., & Le Pichon, X. (1987). Physiography and structure of the western Iberian continental margin off Galicia, from sea beam and seismic data. In G. Boillot, E. L. Winterer, A. W. Meyer, et al. (Eds.), *Initial reports of the Ocean Drilling Program, part A*, (Vol. 103, pp. 77–97). College Station, TX: Ocean Drilling Program. https://doi.org/10.2973/odp.proc.ir.103.105.1987

Sibuet, J. C., Monti, S., Lubrieu, B., Mazé, J. P., & Srivastava, S. P. (2004). Carte bathymétrique de l'Atlantique nord-est et du Golfe de Gascogne. *Bulletin de la Société Géologique de France*, *175*(5), 429–442. https://doi.org/10.2113/175.5.429

Sibuet, J. C., Srivastava, S. P., & Manatschal, G. (2007). Exhumed mantle-forming transitional crust in the Newfoundland-Iberia rift and associates magnetic anomalies. *Journal of Geophysical Research*, *112*, B06105. https://doi.org/10.1029/2005JB003856

Sibuet, J. C., Srivastava, S. P., & Spakman, W. (2004). Pyrenean orogeny and plate kinematics. *Journal of Geophysical Research*, *109*, B08104. https://doi.org/10.1029/2003JB002514

Sopeña, A., López, J., Arche, A., Pérez-Arlucea, M., Ramos, A., Virgili, C., & Hernando, S. (1988). Permian and Triassic rift basins of the Iberian Peninsula. In W. Manspeizer (ed.), *Triassic-Jurassic rifting: Continental breakup and the origin of the Atlantic Ocean and passive margins* (chap. 31, 757–786). https://doi.org/10.1016/B978-0-444-42903-2.50036-1

Srivastava, S. P., Roest, W. R., Kovacs, L. C., Levesque, S., Verhoef, J., & Macnab, R. (1990). Motion of Iberia since the Late Jurassic: Results from detailed aeromagnetic measurements in the Newfoundland basin. *Tectonophysics*, *184*(3-4), 229–260. https://doi.org/10.1016/0040-1951(90)90442-B

Srivastava, S. P., Sibuet, J. C., Cande, S., Roest, W. R., & Reid, I. D. (2000). Magnetic evidence for slow seafloor spreading during the formation of the Newfoundland and Iberian margins. *Earth and Planetary Science Letters*, *182*(1), 61–76. https://doi.org/10.1016/s0012-821x(00)00231-4

Stanton, N., Manatschal, G., Autin, J., Sauter, D., Maia, M., & Viana, A. (2016). Geophysical fingerprints of hyper-extended, exhumed and embryonic oceanic domains: The example for the Iberia-Newfoundland rifted margins. *Marine Geophysical Researches*, *37*(3), 185–205. https://doi.org/10.1007/s11001-016-9277-0

Sutra, E., & Manatschal, G. (2012). How does the continental crust this in a hyperextended rifted margin? Insights from the Iberia margin. *Geology*, *40*(2), 139–142. https://doi.org/10.1130/G32786.1

Sutra, E., Manatschal, G., Mohn, G., & Unternehr, P. (2013). Quantification and restoration of extensional deformation along the western Iberia and Newfoundland rifted margins. *Geochemistry, Geophysics, Geosystems*, *14*, 2575–2597. https://doi.org/10.1002/ggge.20135

Talwani, M., & Heirtzler, J. R. (1964). Computation of magnetic anomalies caused by two dimensional bodies of arbitrary shape. In G. A. Parks (Ed.), *Computers in the mineral industries, part 1. Stanford University publications*, *Geological Sciences*, (Vol. 9, pp. 464–480).

Talwani, M., Worzel, J. L., & Landisman, M. (1959). Rapid gravity computations for two dimensional bodies with application to the Mendocino submarine fracture zone. *Journal of Geophysical Research*, *64*, 49–59. https://doi.org/10.1029/JZ064i001p00049

Tavani, S. (2012). Plate kinematics in the Cantabrian domain of the Pyrenean orogeny. *Solid Earth*, *3*(2), 265–292. https://doi.org/10.5194/se-3-265-2012

Thinon, I., Fidalgo-González, L., Réhault, J. P., & Olivet, J. L. (2001). Pyrenean deformations in the Bay of Biscay. *Comptes Rendus de l Académie des Sciences - Series IIA: Sciences de la terre et des planètes*, *322*, 561–568.

Thinon, I., Matias, L., Réhault, J. P., Hirn, J., Fidalgo-González, L., & Avedick, F. (2003). Deep structure of the Armorican Basin (Bay of Biscay): A review of Nargasis seismic reflection and refraction data. *Journal of the Geological Society of London*, *160*, 561–568.

Tucholke, B. E., Sawyer, D. S., & Sibuet, J. C. (2007). Breakup of the Newfoundland-Iberia rift. In G. D. Karner, G. Manatschal, & L. M. Pinheiro (Eds.), *Imaging, mapping and modelling continental lithosphere extension and breakup*, *Special Publications* (Vol. 282, pp. 9–49). London: Geological Society.

Tugend, J., Manatschal, G., & Kusznir, N. J. (2015). Spatial and temporal evolution of hyperextended rift systems: Implication for the nature, kinematics, and timing of the Iberian-European plate boundary. *Geology*, *43*(1), 15–18. https://doi.org/10.1130/G36072.1

Tugend, J., Manatschal, G., Kusznir, N. J., & Masini, E. (2015). Characterizing and identifying structural domains at rifted continental margins: Application to the Bay of Biscay margins and its Western Pyrenean fossil remnants. *Geological Society, London, Special Publications*, *413*(1), 171. https://doi.org/10.1144/SP413.3

Tugend, J., Manatschal, G., Kusznir, N. J., Masini, E., Mohn, G., & Thinon, I. (2014). Formation and deformation of hyperextended rift systems: Insights from rift domain mapping in the Bay of Biscay-Pyrenees. *Tectonics*, *33*, 1239–1276. https://doi.org/10.1002/2014TC003529

Vázquez, J. T., Medialdea, T., Ercilla, G., Somoza, L., Estrada, F., Fernández Puga, M. C., et al. (2008). Cenozoic deformational structures on the Galicia Bank Region (NW Iberian continental margin). *Marine Geology*, *249*(1-2), 128–149. https://doi.org/10.1016/j.margeo.2007.09.014

Vegas, R., Vázquez, J. T., Olaiz, A. J., & Medialdea, T. (2016). Tectonic model for the latest Triassic-Early Jurassic extensional event in and around the Iberian Peninsula. *Geogaceta*, *60*, 23–26.

Wessel, P., & Smith, W. H. F. (1995). *New version of the Generic Mapping Tools (GMT)*. Washington, DC: American Geophysical Union.

Wessel, P., Smith, W. H. F., Scharroo, R., Luis, J. F., & Wobbe, F. (2013). Generic Mapping Tools: Improved version released. *Eos Transactions American Geophysical Union*, *94*(45), 409–410. https://doi.org/10.1002/2013EO450001

Whitmarsh, R. B., Beslier, M. O., & Wallace, J. P. (1998). *Proceedings of the Ocean Drilling Program, initial reports* (Vol. 173). College Station, TX: Ocean Drilling Program.

Whitmarsh, R. B., Pinheiro, L. M., Miles, P. R., Recq, M., & Sibuet, J. C. (1993). Thin crust at the western Iberia Ocean—continent transition and ophiolites. *Tectonics*, *12*, 1230–1239. https://doi.org/10.1029/93TC00059

Whitmarsh, R. B., & Sawyer, D. S. (1996). The ocean/continent transition beneath the Iberia abyssal plain and continental rifting to seafloor-spreading processes. In R. B. Whitmarsh, D. S. Sawyer, & A. Klaus (Eds.), *Proceedings of the Ocean Drilling Program, scientific results, 149* (pp. 713–733). College Station, TX: Ocean Drilling Program. https://doi.org/10.2973/odp.proc.sr.149.249.1996

Whitmarsh, R. B., White, R. S., Horsefield, S. J., Sibuet, J. C., Recq, M., & Louvel, V. (1996). The ocean-continent boundary off the western continental margin of Iberia: Crustal structure west of Galicia Bank. *Journal of Geophysical Research*, *101*, 28,291–28,314.

Wilson, R. C. L., Hiscott, R. N., Willis, M. G., & Gradstein, P. M. (1989). The Lusitanian Basin of west-central Portugal: Mesozoic and Tertiary tectonic stratigraphic and subsidence history. In A. J. Tankard & H. R. Balkwill (Eds.), *Extensional tectonics and stratigraphy of the North Atlantic Margins*, *AAPG Memoirs* (Vol. 46, pp. 341–361).

Won, I. J., & Bevis, M. (1987). Computing the gravitational and magnetic anomalies due to a polygon: Algorithms and Fortran subroutines. *Geophysics*, *52*, 232–238. https://doi.org/10.1029/96JB02579

Ziegler, P. A. (1982). *Geological Atlas of Western and Central Europe* (p. 130). The Hague, Netherlands: Shell International Petroleum, Maatschappij.